DOT/FAA/TC-18/51

Non-Destructive Evaluation Methods for Detecting Major Damage in Internal Composite Structural Components

February 2019

Final Report

U.S. Department of Transportation
Federal Aviation Administration

NOTICE

This document is disseminated under the sponsorship of the U.S. Department of Transportation in the interest of information exchange. The U.S. Government assumes no liability for the contents or use thereof. The U.S. Government does not endorse products or manufacturers. Trade or manufacturers' names appear herein solely because they are considered essential to the objective of this report. The findings and conclusions in this report are those of the author(s) and do not necessarily represent the views of the funding agency. This document does not constitute FAA policy. Consult the FAA sponsoring organization listed on the Technical Documentation page as to its use.

This report is available at the Federal Aviation Administration William J. Hughes Technical Center's Full-Text Technical Reports page: actlibrary.tc.faa.gov in Adobe Acrobat portable document format (PDF).

1. Report No. DOT/FAA/TC-18/51	2. Government Accession No.	3. Recipient's Catalog No.
4. Title and Subtitle NON-DESTRUCTIVE EVALUATION METHODS FOR DETECTING MAJOR DAMAGE IN INTERNAL COMPOSITE STRUCTURAL COMPONENTS		5. Report Date February 2019
		6. Performing Organization Code
7. Author(s) Margherita Capriotti, Hyungsuk E. Kim, Francesco Lanza di Scalea, Hyonny Kim		8. Performing Organization Report No.
9. Performing Organization Name and Address Department of Structural Engineering UC San Diego 9500 Gilman Drive #0085 La Jolla, CA 92093-005 USA		10. Work Unit No. (TRAIS)
		11. Contract or Grant No.
12. Sponsoring Agency Name and Address Federal Aviation Administration, 2200 S 216th St, 3W-450, Des Moines, WA 98198		13. Type of Report and Period Covered Final Report
		14. Sponsoring Agency Code AIR-600

15. Supplementary Notes

The FAA William J. Hughes Technical Center Aviation Research Division COR was Lynn Pham.

16. Abstract

Damage to internal components of composite aircraft structures is not always detectable from external visual inspection. Of interest are "major" damage modes composed of cracks (consisting of significant amounts of fiber breakage) to internal components such as stringers, shear ties, frames, and disbonding-separation of stringers from the skin. Minor damage, such as voids, small disbonds, and delaminations, although detectable by the methods described herein, are not the serious damage modes creating significant loss of load path which are the focus of these methods. Non-destructive evaluation (NDE) methods based on ultrasonic guided waves to determine the existence of major damage to the internal structure could be useful to aid in decisions on whether invasive disassembly of the aircraft parts is needed to further investigate damage state. Skin and stringer major damage modes were successfully detected from exterior-side NDE tests using both contact and non-contact transducers together with a special Multivariate Outlier Analysis signal-processing method. Specific features were extracted for different time-gated wave packets from each test, and these features were used to present receiver operating characteristic curves, which compare the probability of detection to the probability of false alarm. Further study is in progress to detect major damage in other internal structural components, specifically shear ties and C-frames, at low frequencies 20–80 kHz. A mini-impactor that generates broadband frequency excitation was developed and tested for possible use in internal structure cracks detection.

17. Key Words Non-destructive evaluation, Structural health monitoring, Aerospace composite structure, Ultrasonic guided waves, Statistical outlier analysis, Reliable detection of large hidden damage	18. Distribution Statement This document is available to the U.S. public through the National Technical Information Service (NTIS), Springfield, Virginia 22161. This document is also available from the Federal Aviation Administration William J. Hughes Technical Center at actlibrary.tc.faa.gov.		
19. Security Classif. (of this report) Unclassified	20. Security Classif. (of this page) Unclassified	21. No. of Pages 46	22. Price

Form DOT F 1700.7 (8-72)   Reproduction of completed page authorized

TABLE OF CONTENTS

LIST OF FIGURES

LIST OF TABLES

LIST OF ACRONYMS

CWT	Continuous Wavelet Transform
DI	Damage Index
FEM	Finite Element Model
FFT	Fast Fourier Transform
GSE	Ground Service Equipment
HEWABI	High Energy Wide Area Blunt Impact
MOA	Multivariate Outlier Analysis
MSD	Mahalanobis Squared Distance
NDE	Non-Destructive Evaluation
PFA	Probability of False Alarms
POD	Probability of Detection
RMS	Root Mean Square
ROC	Receiving Operating Characteristics
STFFT	Short Time Fast Fourier Transform
UGW	Ultrasonic Guided Wave

EXECUTIVE SUMMARY

Previous FAA High Energy Wide Area Blunt Impact (HEWABI) project tests on composite panels have generated many severe internal structure damage modes of interest, namely "major" damage modes composed of cracks (fiber failure mode) to stringers, shear ties, frames, and disbonding-separation of stringers from the skin. These major internal damage modes have been found to be barely detectable by visual external observation. Quick non-destructive evaluation methods to determine the existence of damage in the internal structure could be useful to aid in decisions on whether invasive disassembly of the aircraft parts is needed to further investigate the damage state.

Impact-tested composite panels from HEWABI projects were experimentally investigated to determine the optimal frequency used for guided wave-based damage detection throughout the complex panel geometry. Skin and stringer major damage modes were successfully detected from the exterior skin side using ultrasonic guided waves (UGWs) with both contact and non-contact transducers with Multivariate Outlier Analysis. Different time-gated wave packets were chosen to extract specific features to present receiver operating characteristic curves that compared the probability of detection (POD) to the probability of false alarm (PFA). Stringer panel damage modes, such as a disbonded stringer, heel crack in stringer flange, and skin crack along stringer, were nearly perfectly detected (high POD with low PFA).

Further study of UGW transmission is in progress to improve the methods presented herein, which includes establishing better phase velocity dispersion curve extraction through gating, windowing, and space-time filtering, and to retrieve group velocity dispersion curves from Continuous Wavelet Transform (CWT) processing. To generate more energetic excitation, a mini-impactor that generates broadband frequency up to 500 kHz has been developed and tested for possible use in the detection of major damage in internal structures, specifically cracked shear ties and C-frames.

Since conventional non-destructive inspection tools, namely existing "off-the-shelf" pulse-echo ultrasound A-scan and C-scan systems, are limited in their detection ability to only detecting damage within the skin and stringer flanges, lab-level equipment were required to be assembled into custom-built systems capable of exciting and receiving over a wide frequency range in order to detect the damage modes of interest within deeper internal structural components, such as frames and shear ties. Such systems, allowing determination of key frequencies most sensitive to damage modes of interest, allow guidance on the development of new "off-the-shelf" type systems tailored to conducting this inspection method.

1. INTRODUCTION

1.1 Motivation

Damage to internal components, such as a cracked stringer or fuselage frame, is not always visually detectable from the aircraft exterior. Such damage can potentially be created by a High Energy Wide Area Blunt Impact (HEWABI) event. HEWABI events typically occur from ground service equipment (GSE) that usually has rubber bumper material intentionally located at the GSE extremities making contact with the aircraft, and are characterized by high loading applied over a large contacting surface area. Certain damage modes, such as cracked frames and shear ties or stringer heel cracks (see Figure 1), are not detectable by conventional one-sided ultrasonic non-destructive evaluation (NDE) methods (e.g., pulse-echo or tap tests) because these approaches are more suitable for finding delamination within the skin or separation of stringer flanges from the skin. Therefore, the detection of major internal damage requires access to the interior side of the fuselage structure. Such inspections can be quite invasive, especially if they involve disassembly of the aircraft interior, and could be a severe unscheduled disruption to an aircraft that is otherwise supposed to be in service.
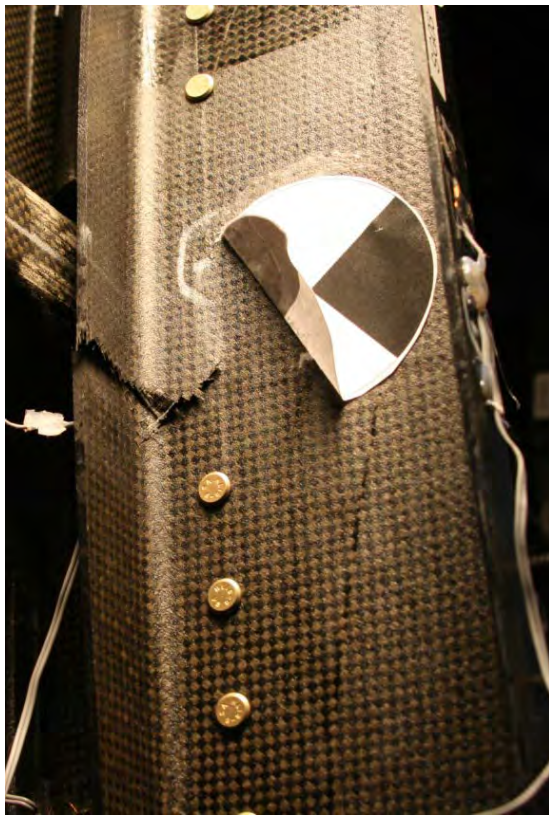
(a) Cracked frame developed in UC San Diego blunt impact specimen frame02 [3]

(b) Crushed Shear Tie
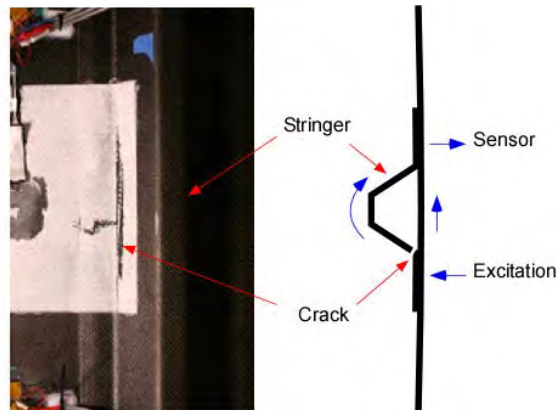
(c) Stringer heel cracks

Figure 1. Internal damage modes of interest: (a) cracked frame developed in UC San Diego blunt impact specimen frame02, (b) crushed shear tie, and (c) stringer heel cracks

A method is therefore needed to quickly and non-destructively determine whether significant-sized internal damage exists (e.g., worse than Category 2 per FAA AC 20-107B definition). This exterior-based inspection would help decide whether an aircraft can be cleared for continued operation, or if a more invasive inspection (and possibly repair action) is needed prior to continued service. Furthermore, this relatively quick inspection method must require access only to the exterior side of the aircraft skin and be achieved while the aircraft is on the ramp. Such an inspection tool is beneficial when suspecting that internal damage might exist, regardless of the source of the damage. It is also highly practical in allowing lower cost, non-scheduled or more regularly scheduled inspections, which do not involve removal of the aircraft interior.

1.2 Objective

To address the need for an inspection method to find major internal damage, this research aims to evaluate NDE methods for finding the presence of major subsurface damage to internal composite fuselage structural members, such as cracks in frames and shear ties [1, 2].

2. TEST SPECIMEN AND PREVIOUS STUDY

2.1 Specimen Fabrication and Impact Damage Formation

Composite panels from the previous FAA HEWABI project [3] developed many major internal damage modes of interest from impact tests. These previously tested composite panels made ideal test specimens for damage-detection studies in the NDE project (currently reported on) because they contained large hidden damage to critical elements. The panels were designed and fabricated by University of California San Diego with supportive guidance from industry experts and were impacted with rubber bumper indenters (see Figure 2) to investigate damage modes induced from a GSE impact scenario.

Composite panels were fabricated using Cytec X840/Z60 12k unidirectional tape and X840/Z60 6k plain weave fabric prepreg materials with ply layups, as listed in Table 1. All parts were laid up by hand at UC San Diego and were autoclave cured at San Diego Composites under a 176.7°C cure temperature. Panels were quasi-statically or dynamically loaded to induce different types of damage from various impact cases. A few of the major damage modes generated are shown in Figure 1.

Table 1. Composite parts layup sequences

Part	Layup	Thickness (mm)	Material
Skin	$[\mathbf{0}/[0/45/90/-45]_{2s}/\mathbf{0}]^*$	2.7	Tape
Stringer	$[[0/45/-45/90/45/-45/0]_{s}/\mathbf{0}]^{**}$	2.4	Tape
Shear Tie	$[45/0]_{3s}$	2.9	Fabric
C-frame	$[45/0]_{3s}^{***}$	2.9	Fabric

* First and last 0° plies are woven fabric
** Last 0° ply is woven fabric
*** Two additional 0° fabric plies were added to flanges
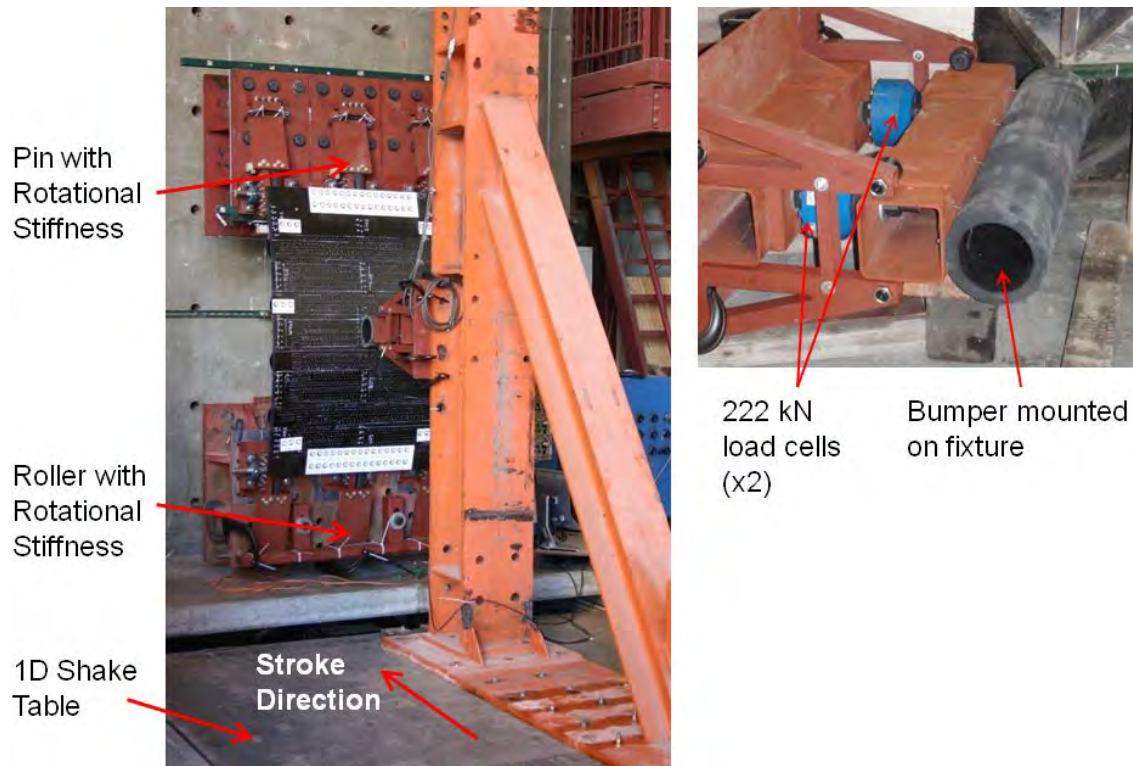
Figure 2. HEWABI project phase I frame panel experimental setup [3]

3. RESEARCH HYPOTHESIS AND APPROACH

3.1 Ultrasonic Guided Wave and Pitch-Catch Method

The previously mentioned composite panels represent very challenging specimens for inspection: their complexity is because of their size, material, shape, and the large number of interfaces (e.g., shear ties fastened to skin, shear ties fastened to frames, stringers co-cured to skin) and components. Ultrasonic guided waves (UGWs) can overcome these problems. They are ultrasonic waves that propagate into prismatic media [4] and build up in specific modes of propagation when interacting with the boundaries of the body. They are able to travel for long distances with low attenuation, allowing wide-area coverage. Common ultrasonic transducers can be employed for both generating and receiving UGW because each structural component supports their propagation, behaving as a "natural waveguide."

Numerical finite element models (FEMs) of the examined composite assembly have been realized in previous studies [5], in which UGW propagation can be observed after an impact excitation; the waveguide behavior of the skin, stringer, shear tie, and C-frame is noticed as the wave travels through and along them (see Figure 3).

3

| (a) 3D view | (b) Cross-sectional view and schematic of wave modes |
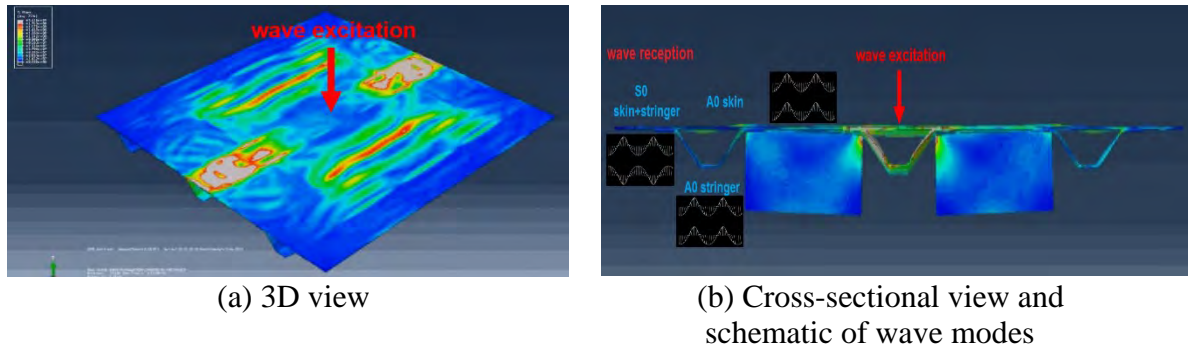
Figure 3. FEM wave propagation: (a) 3D view and (b) cross-sectional view and schematic of wave modes

The characteristic of UGW propagation into multiple wave modes also has to be considered. Two main traveling modes (anti-symmetric A_0 and symmetric S_0 of first order) propagate through the specimen and can be recognized in both FEM simulations and experiments for the examined frequency range (up to 10 kHz for FEM, and 150 kHz for narrowband excitation in the experiments). They travel at different group and phase velocities and exhibit dispersive behavior (i.e., wave velocity is frequency dependent for a given structural arrangement and load path integrity).

The multi-mode and dispersive behavior of UGWs has to be addressed with dedicated signal processing, as explained in the next section, and can be exploited within an NDE perspective after FEM and experiments have shown the presence and interaction of these modes with the structural components and significant states of damage. The guided nature itself of these waves offers the potential of advanced NDE, since the geometry and the material (e.g., boundary conditions and material properties) support the propagation of UGW in specific dispersive manner and guide them into and along the structure. Scattering due to geometrical discontinuities and/or defects of the order of the employed wavelengths reflects into mode-conversion, absorption or enhanced transmission that will affect the recorded waveform. Moreover, employing lower frequency UGWs allows the detection of major damage modes without being attenuated by the multiple interfaces and/or affected significantly by defects that are not structurally critical.

Additional analytical studies and FEM simulations of simple aluminum and composite plates have supported the exploitation of UGW modes and aided the time gating of the signals collected in the tests. Phase-velocity information could be extracted and used to identify the propagating modes, and then related to the structure components and to their pristine or damaged status.

Because of the practical requirement of one-sided external inspection and of wide-area coverage, a pitch-catch approach was chosen for the ability of UGWs to penetrate through the structure's multiple joined parts. As Figure 4 shows, an ultrasonic actuator sends the excitation from the outside skin, and the excited wave propagates through the different components and travels back into the skin where it can be collected from an ultrasonic sensor. The received signal contains information about the overall stiffness and structural integrity of the specimen it traveled through; therefore, energy and time-related characteristics can be extracted and interpreted for the inspection of the covered area.

4
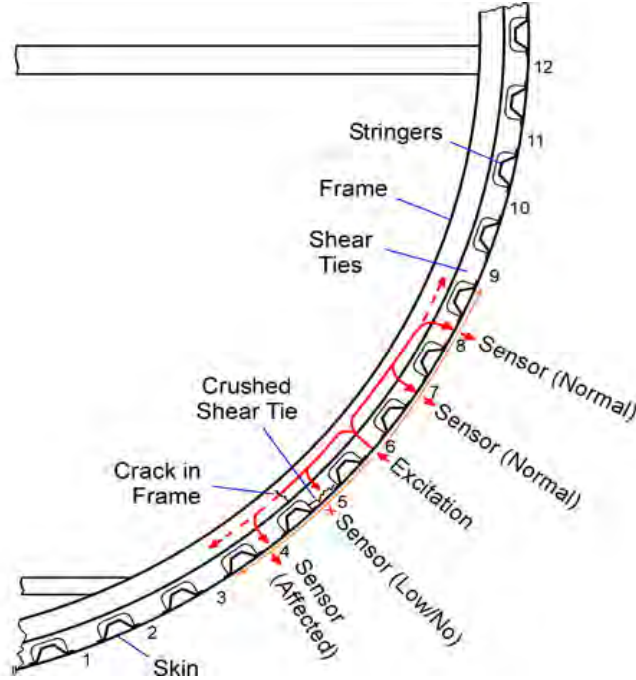
Figure 4. Schematic of pitch-catch approach from outside only

3.2 Signal-Processing Techniques

The collected signals need a combined time and frequency analysis to extract useful information about the UGW propagation and exploit it for damage detection. Specifically, Short Time Fast Fourier Transform (STFFT) and Continuous Wavelet Transform (CWT) were used. These methods divide the signal into successive frames of smaller length and extract their frequency content as a function of arrival time. While the STFFT performs a Fast Fourier Transform (FFT) on each time frame, the CWT applies windows of different sizes to each subsection of the signal—specifically, longer time windows for low frequencies and shorter time windows for high frequencies. This allows a better resolution in the resulting joint time-frequency 2D plot, according to the Heisenberg uncertainty principle [4].

STFFT and CWT are particularly necessary when a multi-mode dispersive wave propagation is involved. This capability can be exploited for group velocity dispersion curve retrieval, reflections, or wave propagation into different component recognition, and damage detection.

A two-dimensional (2D) FFT [6] was also employed for phase velocity dispersion curve extraction. In this case, a multiple receiver or excitation setup was needed to also retrieve phase information, related to the spatial wave propagation parameter (wavelength λ), in terms of wavenumber $k = \frac{2\pi}{\lambda}$. The frequency-wavenumber relation (i.e., dispersion relation) can be extracted and, therefore, the phase velocity is determined as shown in equation 1:

$$c_p = k/\omega \qquad (1)$$

where k is wavenumber and ω is angular frequency (radian/sec).

5

These processing techniques have been tested on data extracted from both FEM and experimental tests of simple aluminum specimens having well-known behavior prior to being applied to the more complex assembled composite specimens.

3.3 Differential Approach and Statistical Outlier Analysis

The complexity of the geometry and material, and the variations due to operational testing conditions, required the use of a differential approach. This method involved an excitation placed in the center between two receivers, co-linearly placed on both sides, which catch the signals after they have traveled into the structure (see Figure 5). The symmetrical configuration picks up any imbalance between the two signals as the presence of an anomaly in the wave path; therefore, a defect or damage can be deduced to exist. The collected signals are affected by reflections, mode conversion, and excitation changes but cannot be used in an absolute manner.
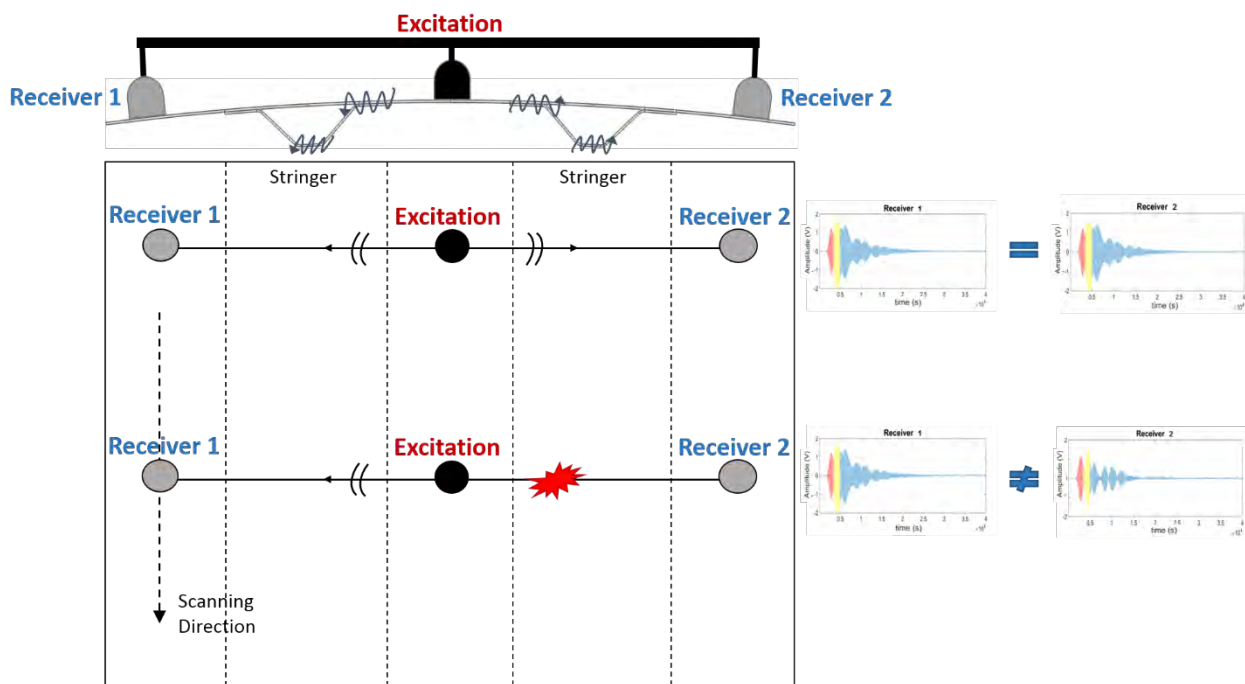
Figure 5. Schematic of differential approach scanning

The need for rapid inspection and the use of UGW testing suggested the use of a line-scanning approach, which can cover a large area in one scan. The panels were scanned along the stringer main axis dimension, inspecting the portion perpendicular to the stringer covered by the transducers. Each line scan becomes a test signal in a B-scan mode (see Figure 5).

This process lends itself to a statistical analysis aimed at minimizing the instability of the signal because of normal operational variability across a scan (e.g., inhomogeneities) and maximizing signal variations due to true structural defects. Following the general statistical Multivariate Outlier Analysis (MOA) for novelty detection [7], the test scans are normalized by their normal statistical distribution. Differences due to the presence of an anomaly in the structure emerge as outliers with respect to the normal distribution, which is built relying on a baseline (i.e., a collection

of signals from a known pristine area of the specimen). The MOA processor computes a damage index (DI) as a metric for defect detection using the Mahalanobis Squared Distance (MSD):

$$DI = (x - \bar{x}) \times C^{-1} \times (x - \bar{x})^T \tag{2}$$

where x is the vector containing features extracted from the test signal, $\bar{x}$ is the vector containing the mean values of the features extracted from the baseline signals, and C is the covariance matrix. The DI is plotted on position axes (see Figure 6a) so that the defective scans can be located in correspondence to a high-DI value with respect to the "low-noise" floor of the baseline areas.

Detailed information on the MOA algorithm will be explained in the results section, referring to the specific cases, because the processor feature extraction is tailored by the test setup and equipment used, and can be adapted toward the desired outcome.

Globally, prior to feature extraction, time gating is performed to select the wave packets on which the statistical analysis needs to focus. The choice of the time gates relies on the physics of the multi-mode wave propagation into the panel components and is based on the velocity information extracted from the FEM simulations.

Finally, the damage detection performance of the technique needs to be assessed. For this purpose, receiving operating characteristics (ROC) curves (see Figure 6b) were computed for a quantitative evaluation of the technique, and a practical metric for the user to understand and choose the achievable tradeoff in the damage-detection phase, and to further assist in the decision-making process. For each defect type, at varying DI thresholds, the probability of detection (POD) was computed as a function of the probability of false alarms (PFA). A ROC curve located in the top left corner of the plot and an area under the curve very close to 1 are indicative of a good detection performance. A 1:1 slope line in the ROC graph indicates a random guess.
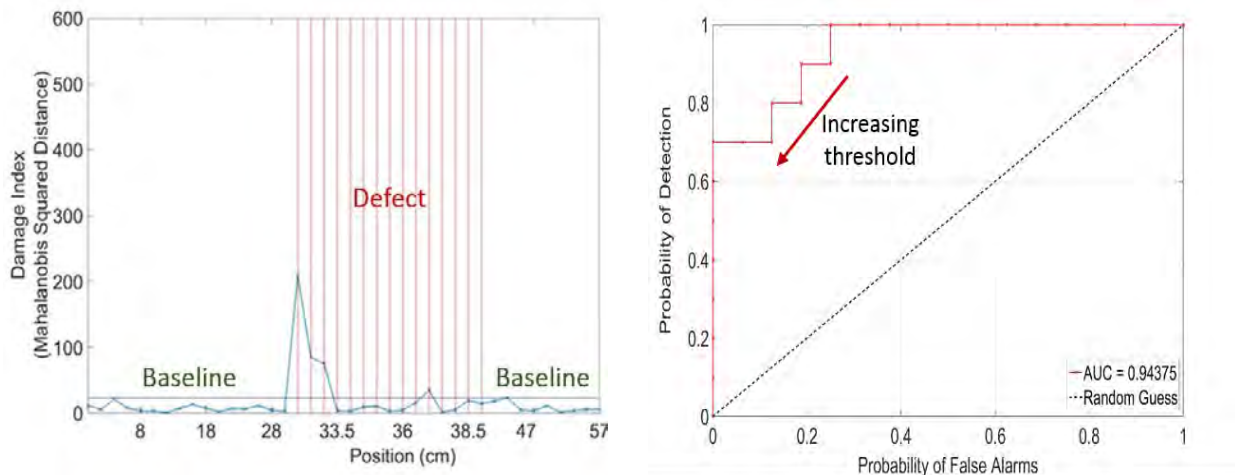
(a) DI plot   (b) ROC curve

Figure 6. Schematic of damage detection analysis: (a) DI plot and (b) ROC curve

4. RESULTS

4.1 Initial UGW Test: Damage Interaction

Initial UGW tests were performed on test specimen Frame02, which had flange cracks on the C-frame, different damage severities on the shear ties, and crack damage on the stringer. The aim of these tests was to observe if it is possible to distinguish damage presence from transmitted wave outputs when differential comparison is made between a damaged versus undamaged wave path. PICO sensors from MISTRAS Group, Inc. with a broad frequency bandwidth were used to find an optimal frequency range for wave propagation through the composite panels. A Piezo Linear Amplifier was used to amplify the actuator transducer, and Olympus Preamplifiers (Model 5660C) were used for received signal gain.

For the pitch-catch detecting method shown in Figure 4, the frequency range below 200 kHz was experimentally determined to deliver strong wave transmission through the panel for the distance of 305 mm between the actuator and the receiver. Frequency sweep tests below 200 kHz were performed on each subcomponent of the panel, specifically C-frames and shear ties, to study changes in UGW data output when waves propagate through damaged components in comparison to pristine components.

First, the C-frames were tested and compared, as shown in Figure 7. UGWs were excited and received at two symmetrical distances—305 mm to the left and right of the excitation—along the span of the C-frame where the shear ties are joined via bolts to the C-frame. Tests were performed on a pristine C-frame and on an impact-damaged C-frame for the wave-alteration comparison in which the UGWs interact with damage on the C-frame.

(a) Pristine C-frame   (b) Impacted C-frame with through-the-flange crack
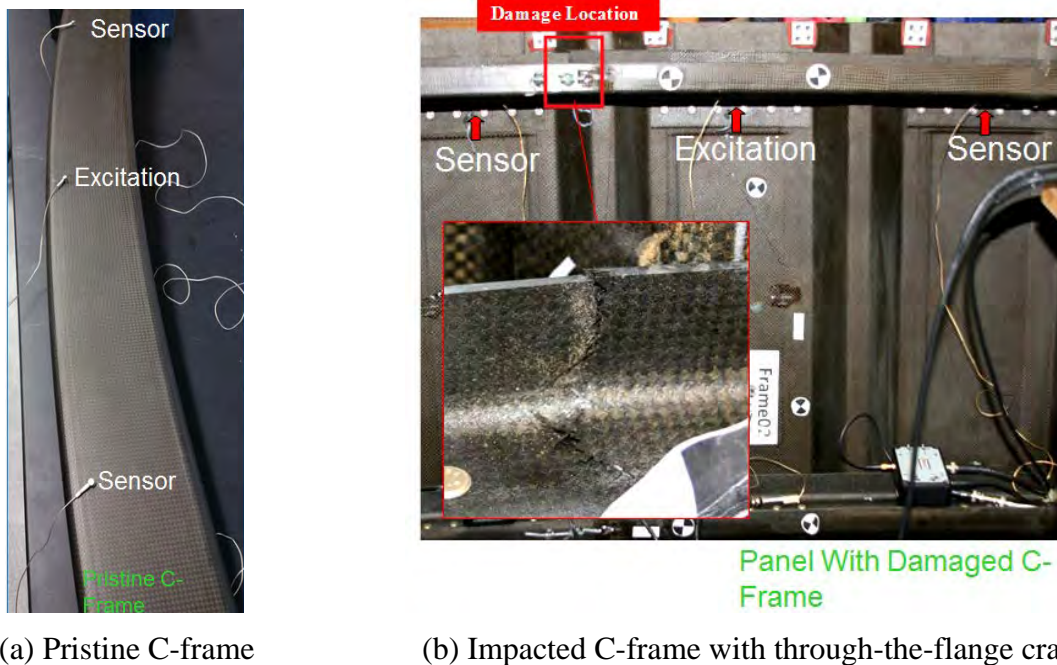
Figure 7. Initial C-frame UGW test setup: (a) pristine C-frame and (b) impacted C-frame with through-the-flange crack

For excitation, a five-cycle Hanning windowed sine tone burst signal was generated through a built-in Arbitrary Waveform Generator on the PicoScope 4824. The Piezo Linear Amplifier amplified the excitation signal, and the received signals were averaged for an improved signal-to-noise ratio. Experimental results in Figure 8a show a small variance in left versus right measurements for the pristine C-frame due to the splice joined layup in the C-frame. Figure 8b shows a much more noticeable difference in FFT amplitude due to significant attenuation in UGW of nearly 55% when the wave interacts with the flange damage on the C-frame (see Figure 7b).

(a) Pristine C-frame   (b) C-frame with through-the-flange crack
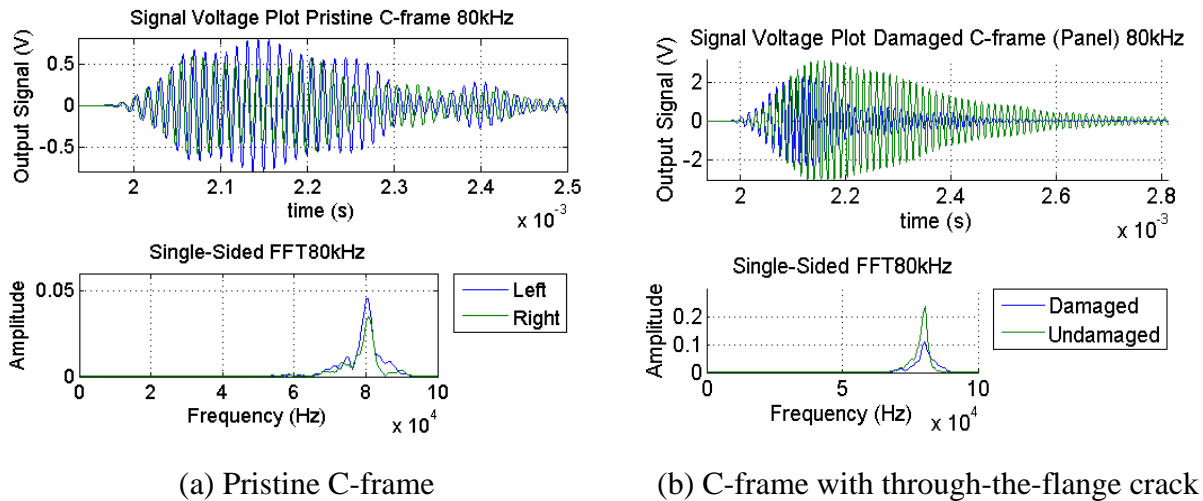
Figure 8. Initial C-frame UGW test result comparison: (a) pristine C-frame and (b) C-frame with through-the-flange crack

Second, shear ties with different damage severity from the Frame02 panel were investigated to understand wave attenuation through shear tie cracks (see Figures 9c, d, and e). For this experiment, the same method of excitation as the C-frame test was generated from the exterior skin, where the shear ties are joined to the skin via countersunk bolts (see Figure 9a). Receiver sensors were located on the C-frame to collect UGWs propagating through the shear tie (see Figure 9b). The actuator and receivers for this test were Mistras R15s transducers with a narrowband frequency and 150 kHz resonance. These tests showed differences in the transmitted waves through different damage levels in the shear ties. Figures 10a and 10b show the comparison of UGW test results for a shear tie at 50 kHz and 150 kHz excitation, respectively. Comparing A_0 mode time-gated wave results between shear tie 11 (pristine) and shear tie 06 (partial corner crack), 150 kHz tests show a higher UGW attenuation of approximately 78%, whereas 50 kHz tests showed lower attenuation of 18% due to the presence of damage. A higher frequency appears to be more suitable to detect damage, but it was found that UGW frequencies higher than 80 kHz do not propagate very efficiently through the internal structure as compared to the exterior skin propagation (see section 4.2.3 "Conjoined Stringer Panels").
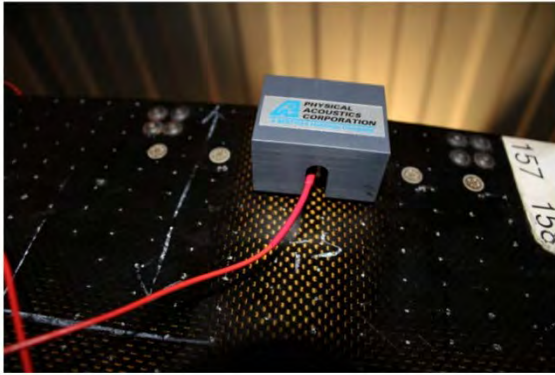
(a) R15s transmitter fixed on exterior skin
using magnetic hold down
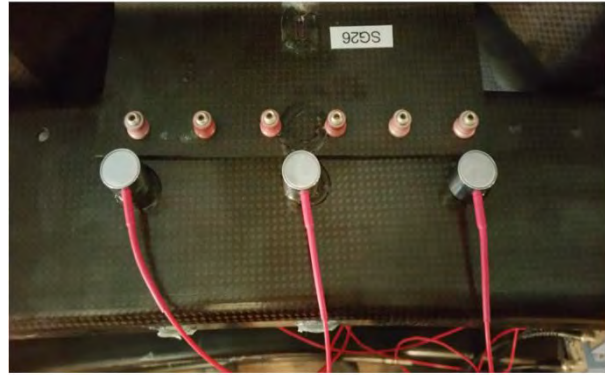
(b) R15s receivers on C-frame

(c) Undamaged shear tie for
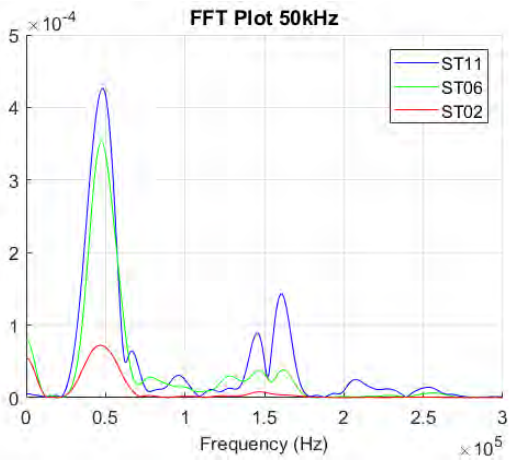baseline (ST11)

(d) Partially cracked shear tie
at the corner (ST06)

(e) Complete crack along the
bolt lines (ST02)

Figure 9. Shear tie test setup: (a) R15s transmitter fixed on exterior skin using magnetic hold down, (b) R15s receivers on C-frame, (c) undamaged shear tie for baseline, (d) partially cracked shear tie at the corner, and (e) complete crack along the bolt lines
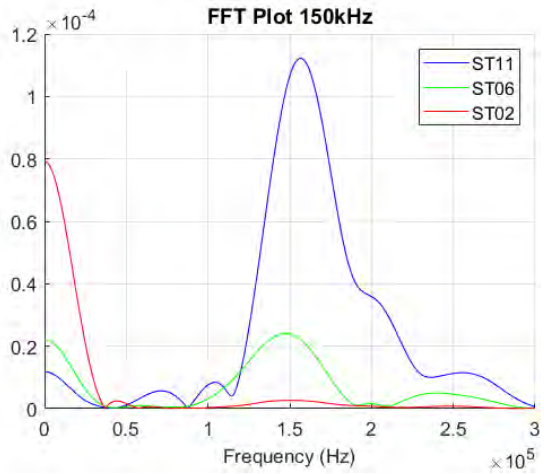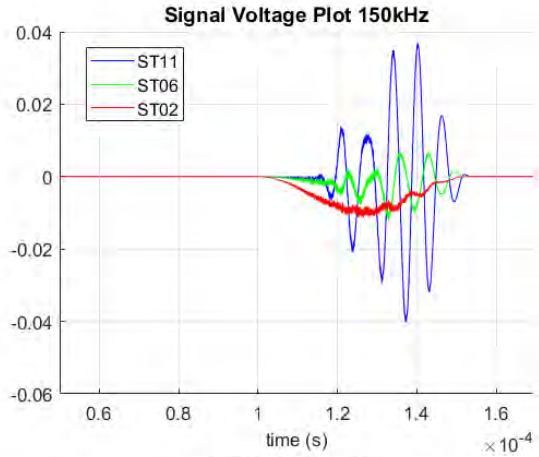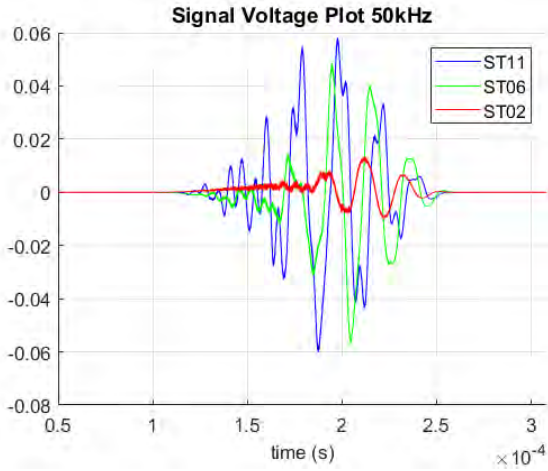
(a) Signal and FFT result 50kHz   (b) Signal and FFT result 150kHz

Figure 10. Shear tie test results comparison: (a) signal and FFT result 50 kHz and (b) signal and FFT result 150 kHz

4.2 Wave Propagation in Internal Components

Although wave propagation through each individual internal component was studied, differentiating between stiffened internal structure wave transmission versus skin wave transmission remained challenging. The complex assembly of the panel affects the wave propagation scattering pattern and transmission through multiple wave paths. It is very important to note that UGWs are excited and received from external skin of the mechanically fastened region of the panel and waves propagate through unique wave paths, (skin, skin with stringer, and shear tie with C-frame) before receiver sensor acquires signals from multiple paths, as described earlier in section 3. Therefore, various levels of assembly and aspects of joining were further investigated to establish their influence on UGW transmission.

4.2.1 Assembling and Disassembling of the Structure

Tests performed with Frame02 panel subcomponent parts assembled and disassembled helped to understand wave energy leakage into the internal structural components versus transmission within the skin only. UGW tests were performed first on the full assembly (skin with C-frame bolt joined by shear ties), then again after removal of the C-frame only, and finally again after the removal of shear ties (see Figure 11). Transducers were consistently fixed in place throughout these assembly and disassembly tests using a 3D-printed hold-down mount, as seen in Figure 11d. Figure 12 shows UGW test results at 150 kHz and the intensity increase for each disassembled part: a 43% increase when only the C-frame was disassembled, and a 63% increase when the shear ties were disassembled for skin-only wave propagation. Test results could be related to how much energy was drawn into the internal composite stiffening components. It was noted that 86% of the energy leaked into the internal structure when the skin-only wave energy was compared to the fully assembled panel.
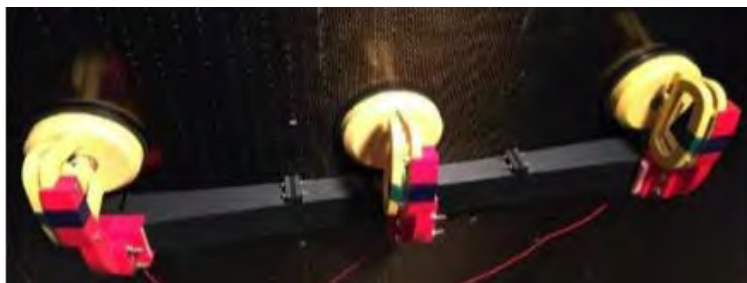
(a) Full assembly with C-frame and shear ties

(b) C-frame only removed (shear ties mounted)

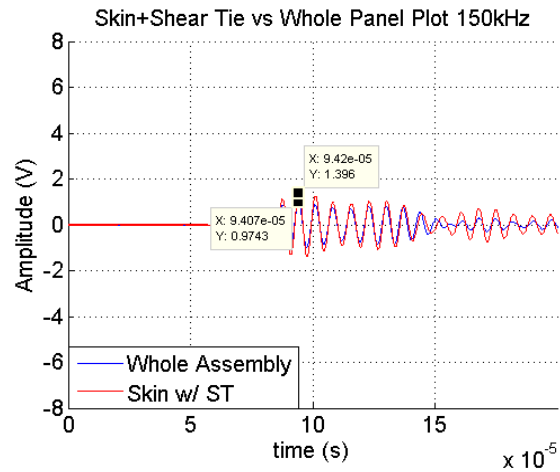(c) C-frame and shear ties removed (co-cured shims visible on skin)

(d) 3D-printed hold-down mounts for transducers on outer skin

Figure 11. Different levels of disassembly for UGW tests: (a) full assembly with C-frame and shear ties, (b) C-frame only removed, (c) C-frame and shear ties removed, and (d) 3D-printed hold-down mounts for transducers on outer skin
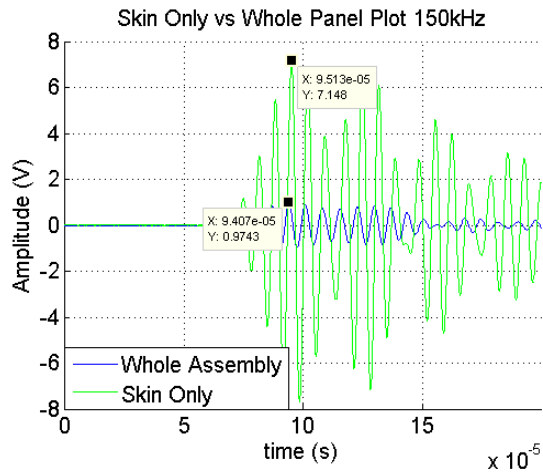
(a) Skin-only vs. whole assembly   (b) Skin and shear ties vs. whole assembly

Figure 12. Assembling/disassembling test results: (a) skin-only vs. whole assembly and (b) skin and shear ties vs. whole assembly

4.2.2 Bolted-Joint Wave Propagation

From the previous Frame02 panel assembly and disassembly experiments, originally bolted Hi-Lok[TM] collars were replaced with common industry nuts to allow for easier assembly, disassembly, and adjustment of the fastening torque level. Nuts were tightened back to the same torque of 7.9 N-m applied to the Hi-Lok[TM] collars (HL70-8), and wave transmission through various bolt torque levels were compared. The same test setup was used as in Figures 9a and 9b; bolt torque levels of 2.2 N-m and higher did not have much influence on wave transmission through the bolt-joined composite skin to C-frame for frequencies of 150 kHz and lower (see Figure 13a). For frequencies of 150 kHz and lower, experiments showed a slight drop in the UGWs amplitude as the torque level went beyond certain strengths for each swept frequency. UGW transmission through bolt-joined aluminum plates in an experiment by Bao et al. [8] shows a similar behavior at 320 kHz, in which measurements showed a slight amplitude decrease at 2.7 N-m torque compared to 2.3 N-m.

14
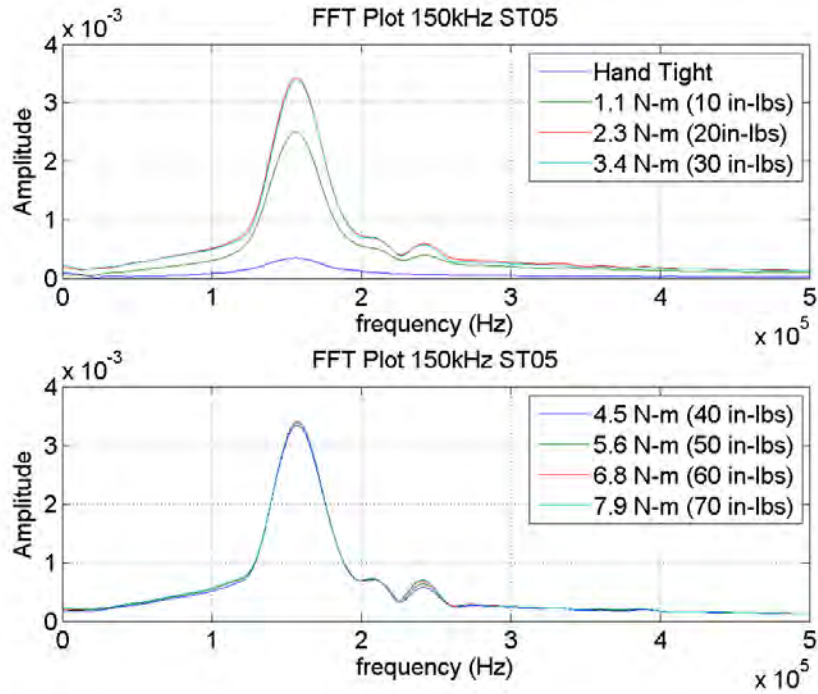
(a) Bolted-joint difference torque wave transmission at 150 kHz
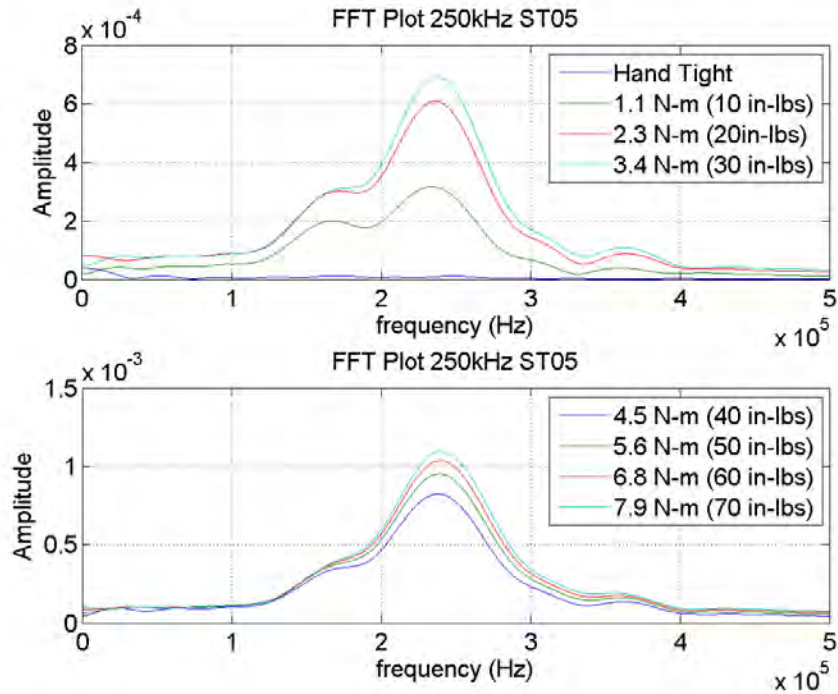
(b) Bolted-joint difference torque wave transmission at 250 kHz

Figure 13. Bolted-joint test results: (a) bolted-joint difference torque wave transmission at 150 kHz and (b) bolted-joint difference torque wave transmission at 250 kHz

However, bolt torque level difference had a significant effect on wave transmission as frequency increased above 150 kHz; every increment of torque level up to 7.9 N-m showed a difference in wave-transmission intensity at 250 kHz (see Figure 13b). Bolt-joined composite parts have a rough surface compared to the aluminum surface, and minor changes in wave-transmission energy at different bolt torque levels (i.e., clamp-up between joined parts) are estimated to show at different frequencies because of the surface finish. These results show that bolt torque affects wave transmissions, which are found to be frequency-dependent for higher frequencies, and also that under-torqued bolts particularly can strongly alter the NDE results. This validates ultrasonic wave-based loose bolt detection method studied by Yang and Chang [9], where torque level was predicted from attenuation pattern. An application of this is the monitoring of bolt torque loss in composite joints over the course of long-term service, which could result in reduced performance.

4.2.3 Conjoined Stringer Panels

Although the assembly and disassembly test showed that a significant amount of energy leaks into the internal structure, it was still unclear how much of the internally transmitted waves transfer out back to the skin side. To investigate wave transmission through the internal structure only, two smaller stringer panels were joined by a single C-frame, leaving a break in the skin (see Figure 14). By conjoining two panels, skin discontinuity exists and only the waves transmitted through the internal components (through the frame) arrive at the receiver transducer. As seen in Figure 14, the transmitter and receiver attach to the skin on each panel at the center of each shear tie. For a better comparison of the internally transmitted UGW behavior at different frequencies, UGW test results from Pico Sensors (the transmitter and the receiver) were investigated instead of the narrowband frequency R15s sensors. Figure 15 shows that the UGWs transmitted through the internal structure at 50 kHz had much higher energy than the UGWs at 150 kHz. Similarly, additional frequency sweep test results show frequencies lower than 80 kHz give a strong internal wave energy transmission. Therefore, it would be best to use an excitation frequency lower than 80 kHz to better investigate UGW propagation through the internal components (through shear ties and frames), which is a necessary condition for detecting damage in those components.
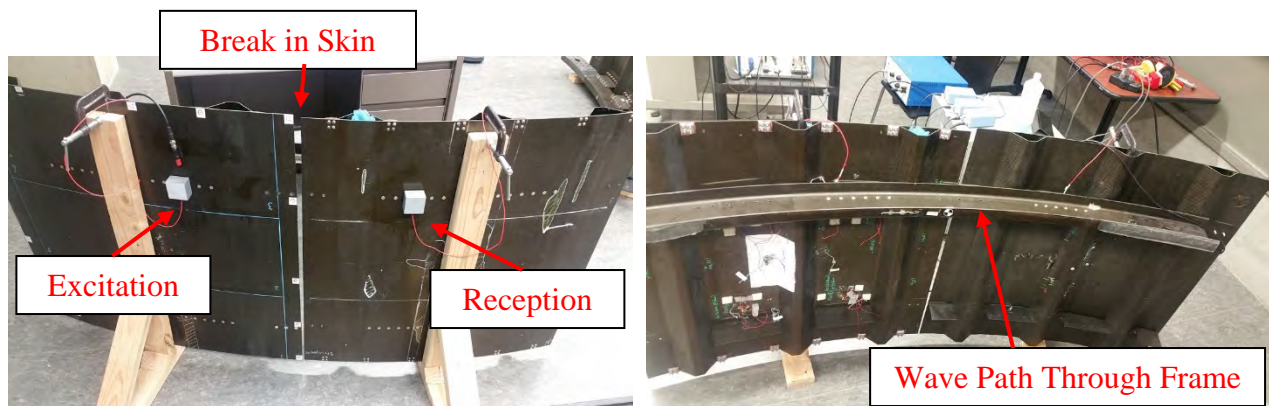
**Figure 14. Conjoined stringer panels**
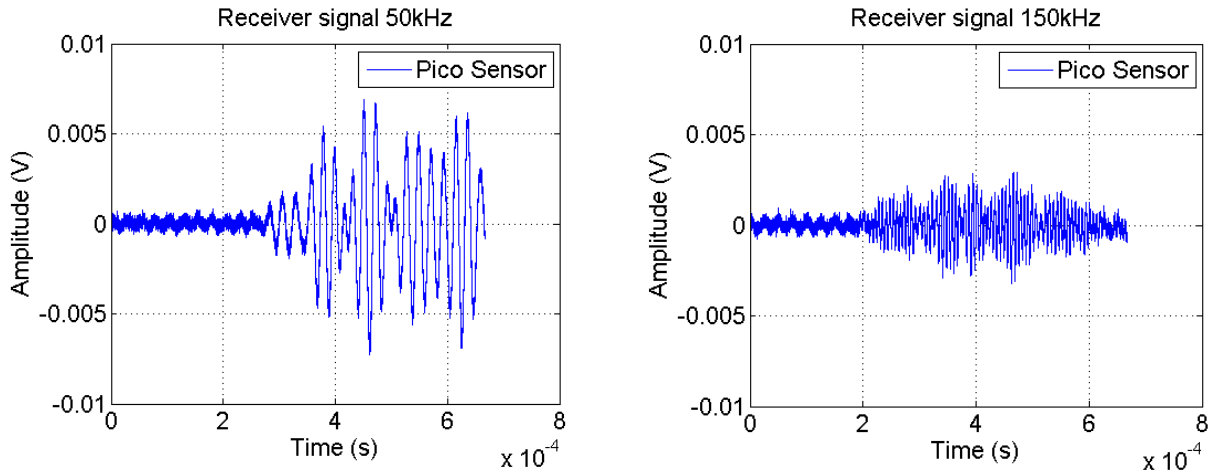
Figure 15. Conjoined stringer panels result

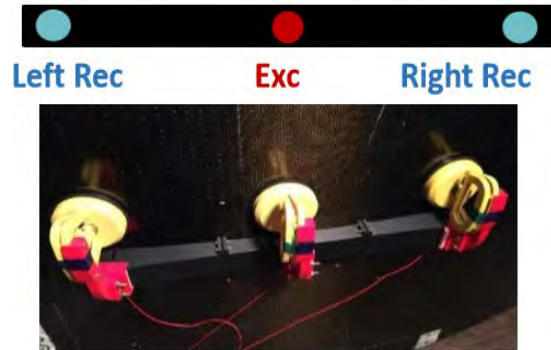## 4.3 Contact-Based Defect-Detection Technique

The development of the UGW-based NDE technique first employed contact PZT transducers. These results, presented in this section, show proof of concept. However, aspects related to contact consistency remain. Therefore, non-contact transducers were also found to be more successful as presented in section 4.4.

4.3.1 Test Setup

Building on what was learned in the previous studies, and to enable inspecting across long distances while penetrating multiple interfaces in a composite material, Mistras R15s narrowband PZT contact transducers were centered at 150 kHz (one for actuation and two for reception). Conventional ultrasonic gel couplant was used, and the differential approach was employed (see Figure 16) to compensate for coupling variations and other changes not associated with damage. Scans performed on the structure across two stringers, as the schematic in Figure 16 shows, used a 3D-printed sensor hold-down mount for consistent contact pressure.
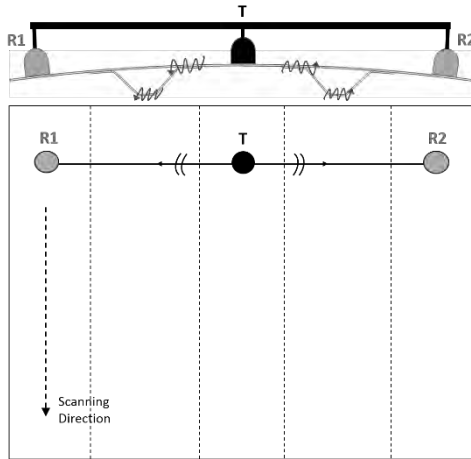
(a) Schematic   (b) Test setup

Figure 16. Contact defect-detection technique: (a) schematic and (b) test setup

The scanning resolution along the panel stringer direction was nominally 2 cm and increased to 0.5 cm and 1 cm near defects. A five-cycle tone burst with Hanning modulation at 150 kHz constituted the excitation signal. Both actuation and reception were controlled by a National Instruments® (NI) PXI unit, running under LabVIEW, performing both excitation and data acquisition.

4.3.2 Damage Detection

After scanning the area of interest, the data post-processing was done using Matlab. Every test signal was time-gated in five possible wave packets exploited in different ways and combinations, as shown in Figure 17 (see packets 1–5).
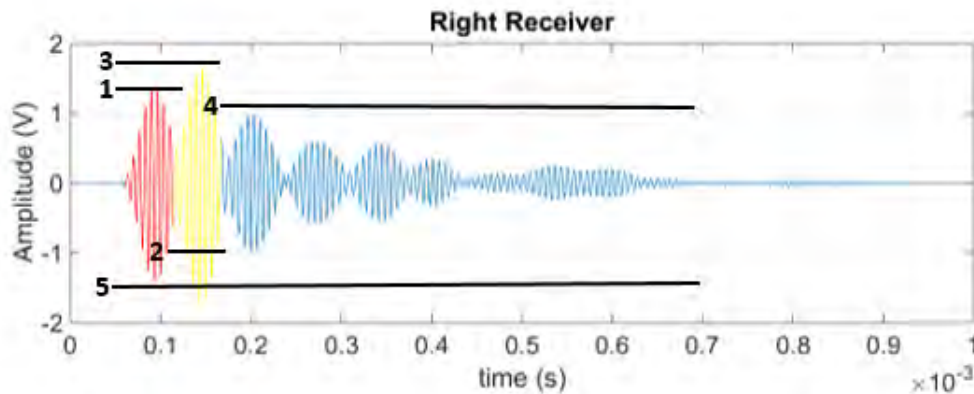
**Figure 17. Typical signal from contact technique with gated wave packets**

Energy-based features were extracted from the selected wave packet, and a comparison between the two opposite receivers (i.e., between R1 and R2 in Figure 16a) was performed by the processor. Table 2 lists the features used. The features contributed to a feature vector that helped to compute the DI according to the MSD for every scan position.

Table 2. Contact technique features list

Feature #	Feature Name	Feature Extraction
1	RMS ratio	$\dfrac{RMS(x_1)}{RMS(x_2)}$
2	Maximum value ratio	$Max\left(\dfrac{Max|x_1|}{Max|x_2|}, \dfrac{Max|x_2|}{Max|x_1|}\right)$
3	Area under packet ratio	$\dfrac{Area(x_1)}{Area(x_2)}$
4	Peak to peak normalized difference	$\dfrac{|Ppk(x_1) - Ppk(x_2)|}{\sqrt{Ppk(x_1) \times Ppk(x_2)}}$
5	Area under FFT normalized difference	$\dfrac{|AreaFFT(x_1) - AreaFFT(x_2)|}{\sqrt{AreaFFT(x_1) \times AreaFFT(x_2)}}$
6	Maximum value cross-correlation normalized difference	$\dfrac{Max(xcorr(x_1, x_2))}{\sqrt{Max(xcorr(x_1)) \times Max(xcorr(x_2))}}$
7	Variance normalized difference	$\dfrac{|Var(x_1) - Var(x_2)|}{\sqrt{Var(x_1) \times Var(x_2)}}$
8	RMS normalized difference	$\dfrac{|RMS(x_1) - RMS(x_2)|}{\sqrt{RMS(x_1) \times RMS(x_2)}}$

The results shown in Figure 18 used the first wave packet in which the colored vertical lines represent the defective areas. The DI increased in correspondence with the detected cracked skin, stringer damage, and detached stringer from skin. The DI was correctly found to be very low for pristine locations.
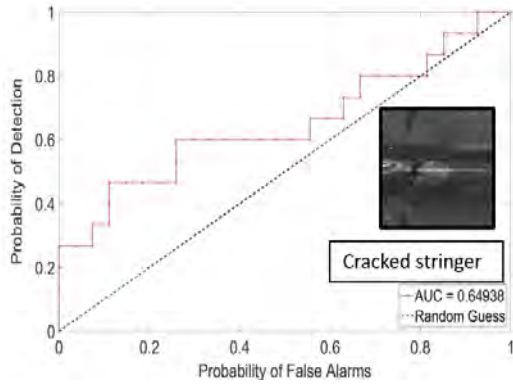
(a) Panel 1   (b) Panel 2
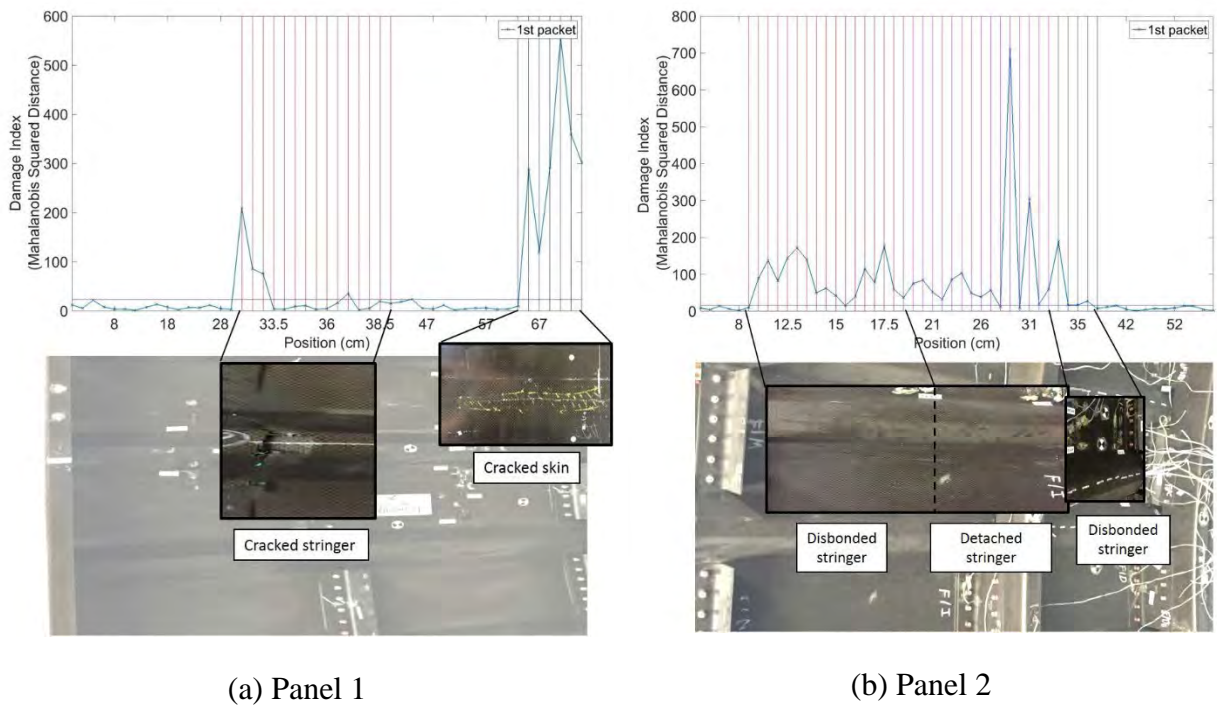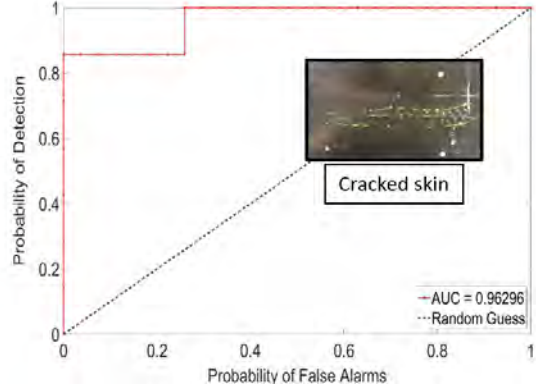
Figure 18. Contact defect-detection technique DI

4.3.3 ROC Curves

The performance of the contact-based defect-detection technique was assessed with the ROC curves for Panel 1 (Frame02) and Panel 2 (Frame01), as shown in Figure 19. The disbonded stringer represents an internal disbond of the stringer from the skin, whereas the detached stringer represents a more severe detachment of the stringer from the skin.

For Panel 1, the defect detection of the cracked stringer was achieved with a POD of 60% and 25% of PFA (see Figure 19a). This "ok" quality of detection was because of the size and orientation of the defect and the use of the first wave packet in the signal for the MOA. The S_0 mode was dominated by an in-plane displacement component that did not penetrate the structure as much as the A_0 mode. Especially for defects existing within the internal components, the S_0 mode was not well-suited and other modes are preferred. The detection of this kind of defect can be improved by focusing the analysis on an anti-symmetric mode and using sensors that are more sensitive to the out-of-plane displacement. The cracked skin defect detection achieved a very good performance, with a 86% POD and 0% PFA or a 100% POD, accepting a 26% PFA (see Figure 19b). This result confirmed the sensor sensitivity and the wave packet interaction with different defects at different locations within the structure and positioned at different orientations with respect to the scanning direction.
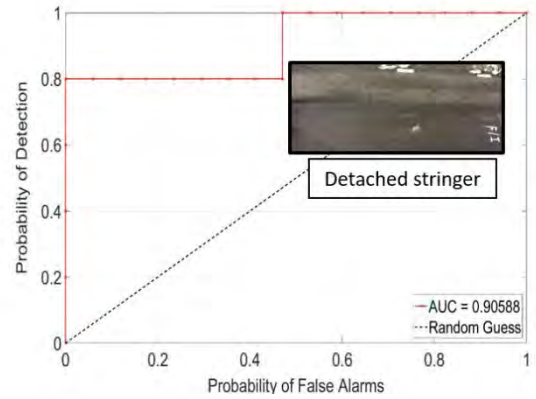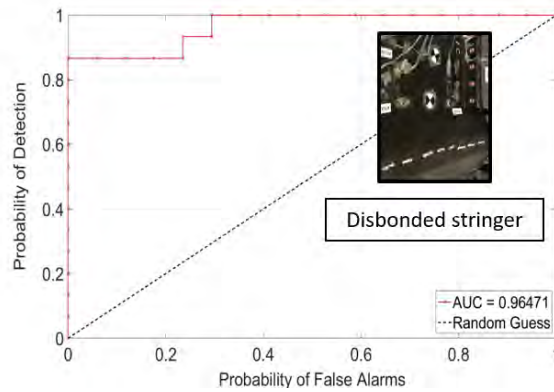
(a) Cracked stringer (Panel 1)

(b) Cracked skin (Panel 1)
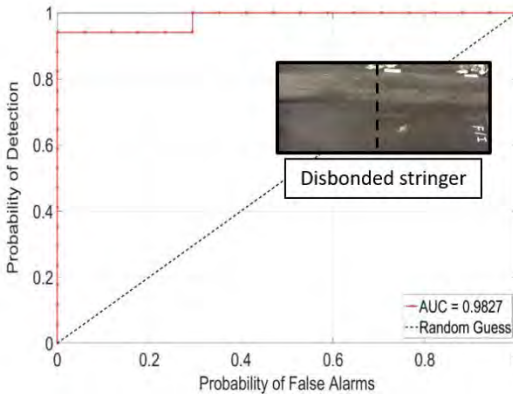
(c) Disbonded stringer (Panel 2)

(d) Detached stringer (Panel 2)

(e) Disbonded stringer (Panel 2)

Figure 19. Contact defect-detection technique ROC curves for various defect types: (a) cracked stringer, (b) cracked skin, (c) disbonded stringer, (d) detached stringer, and (e) disbonded stringer

For Panel 2, all the stringer defects were detected with a very good performance: the disbonded stringer defect can be detected with a 94% POD and 0% PFA or, alternatively, with a 100% POD and 29% PFA (see Figure 19c). A worse performance was found for the detached stringer defect, in which an 80% POD results in a 0% PFA, and a 100% POD results in a 47% PFA (see Figure 19d). The lower disbonded stringer was also detected with an 87% POD with 0% PFA or a 100% POD with 29% PFA (see Figure 19e). The latter two defects were located very close to the shim and bolted part of the panel. The performance is likely affected by the different wave propagation in this area, which could be improved with implementation of an adaptive baseline.

4.4 Non-Contact Based Defect-Detection Technique

Toward a more field applicable solution that is not sensitive to variations in transducer coupling contact-quality, design of a second version of the prototype included use of non-contact (air-coupled) PZT transducers.

4.4.1 Test Setup

A cylindrically focused air-coupled transmitter (NCG200-S50-C76-EP-X, Ultran) and an unfocused air-coupled receiver (NCG200-S19, Ultran) operated in a pitch-catch mode. The transducers (both narrowband with a central frequency of 170 kHz) were mounted on a moving cart, with an appropriate orientation angle according to Snell's law and focus distance given by the manufacturer, which allowed the rapid and consistent scanning (see Figure 20).

(a) Schematic   (b) Test setup
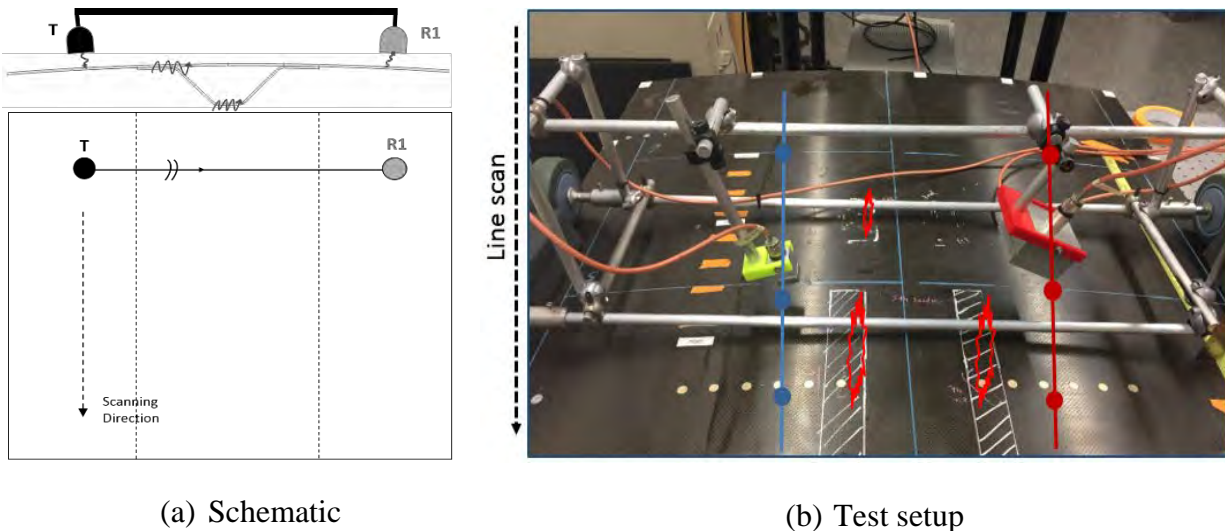
Figure 20. Non-contact defect detection technique: (a) schematic and (b) test setup

In this configuration, the test scanned across one stringer along the same main stringer dimension in a faster process, and with no need for the differential approach because of the improved signal stability. This avoided the need for coupling and eliminated the variation of the excitation strength, which had no influence from the contact pressure exerted by an operator. The new configuration used the same NI PXI unit running on a similar LabVIEW routine. An amplifier provided the necessary increased excitation power (200 V) and pre-amplifiers connected to the receiver also supported the test setup.

4.4.2 Damage Detection

It was possible to isolate, with the aid of the previously extracted wave propagation and velocity information, the S_0 and A_0 modes, penetrating into the skin and into the stringer, as shown in Figure 21.
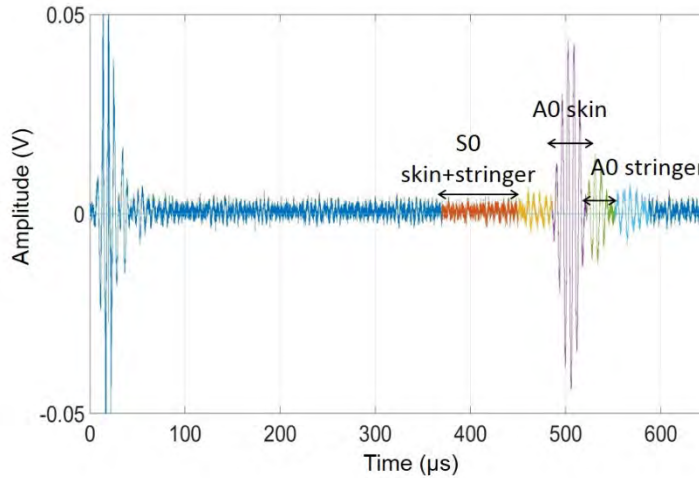
**Figure 21. Typical signal from non-contact technique with gated wave packets**

The MOA algorithm was then modified to accommodate for this additional information by building a feature "super-vector" that allowed for mode selection and mode compounding. The extracted energy and time-based features are listed in Table 3.

Table 3. Non-contact technique features list

Feature #	Feature Name	Feature Extraction
1	Maximum value	$Max\|x_p\|$
2	Index of maximum value	$Ind(Max\|x_p\|)$
3	Variance	$Var(x_p)$
4	Kurtosis	$Kurt(x_p)$

Figure 22 shows the DI test results in terms of MSD, computed and plotted along the scanning positions for the Stringer03 Panel.

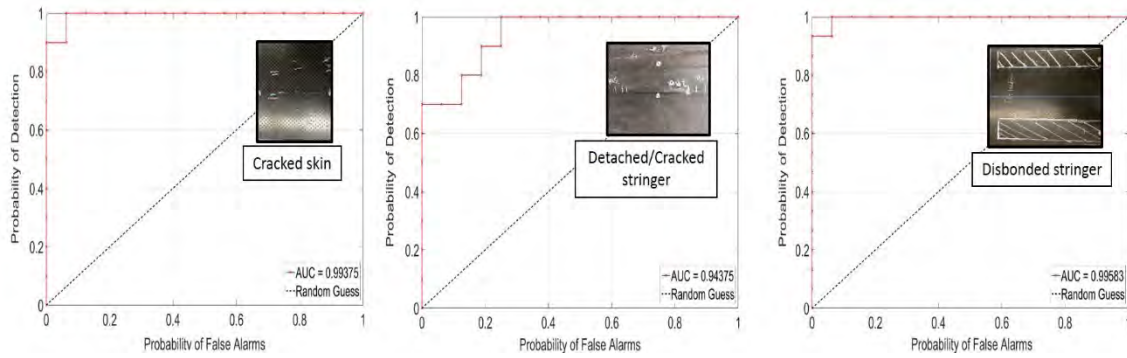(a) Skin-only modes   (b) Skin and stringer modes
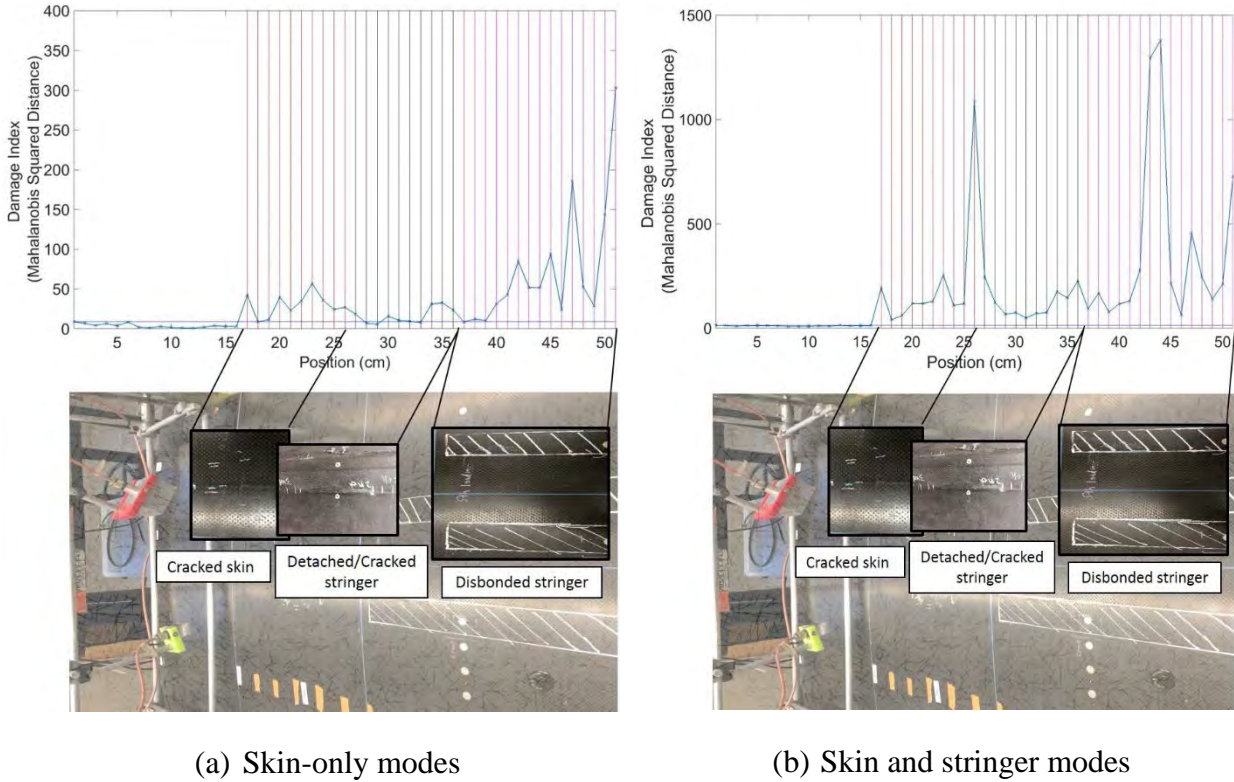
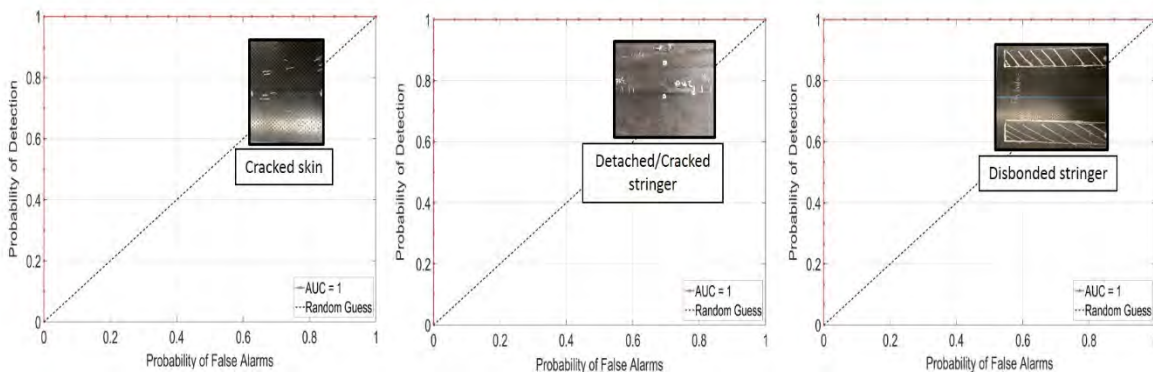**Figure 22. Non-contact defect-detection technique DI: (a) skin-only modes and (b) skin and stringer modes**

It is worth noting the different DI results when using only the skin modes information. In the first case, the skin-only modes, damage detection found skin and stringer defects, but had limited detection of the detached/cracked stringer (a lower level damage), as shown in Figure 22a. The disbonded stringer, although categorized as a stringer damage, showed up much better in the skin-related modes because the stringer disbond affected the related wave propagation, which forced the waves to travel along the surface skin with a higher amplitude, and the stringer absorbed little energy. When adding the stringer modes (the second case) into the MOA processor, the overall detection improved: the deeper stringer defect showed a DI increase with respect to the baseline and the overall DI trace had a higher SNR with respect to the "noise floor" corresponding to the pristine area, as shown in Figure 22b.

4.4.3 ROC Curves

The performance assessment of the non-contact defect detection technique includes the ROC curves for Stringer03 Panel (see Figure 23). The technique performance was very good when using only skin modes (see Figure 23a). The cracked skin and the disbonded stringer defect achieved a 100% POD with less than 10% PFA and a worse performance for the detached/cracked stringer defect (e.g., 100% POD with 25% PFA or 70% POD with 0% PFA). The results improved dramatically when adding stringer mode wave-propagation content (see Figure 23b), reaching a perfect detection for all defect types (100% POD with 0% PFA).

(a) Only Skin modes

(b) Skin and stringer modes

Figure 23. Non-contact defect-detection technique ROC curves for various defect types: (a) only skin modes and (b) skin and stringer modes

4.5 High-Intensity Wave Transmission Through Internal Structure

To have a significant amount of wave energy transmitted through the internal structures comparable to skin-propagated wave energy, a frequency less than 80 kHz is optimal based on the previous conjoined stringer panels experiment. Development of a mini-impactor helped to generate high-energy broadband frequency excitation that can penetrate better into the internal structure. An additional benefit of higher energy excitation is less (or no) amplification of the received signals and higher signal-to-noise ratio. The mini-impactor was manufactured from a unidirectional carbon fiber composite strip body with a metal tip, as shown in Figure 24.
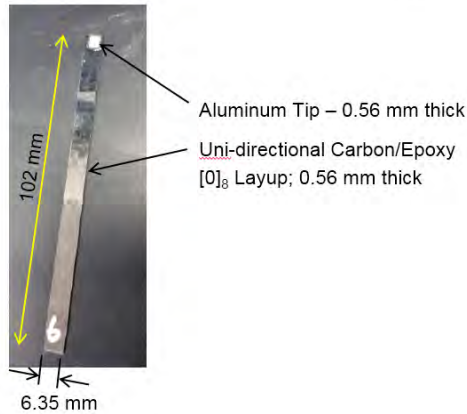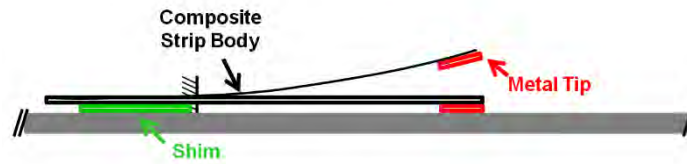
(a) Mini-impactor structure   (b) Impact exertion

Figure 24. Mini-impactor: (a) mini-impactor structure and (b) impact exertion

Studies of the frequency range of the mini-impactor excitation included both a FEM simulation and experiment. The FEM simulation studied the frequency range when various thicknesses of the metal tip impacted an aluminum plate. For impact excitation, the wave simulation used impact from a square metal tip with thickness ranging from 0.5–1-mm thickness traveling at a velocity of 6 m/s onto the aluminum plate. Figure 25 shows metal-tip impact simulation results that generated in-plane waves with a broad range of frequency content from near DC to 800 kHz with varying frequency peaks from 200–300 kHz and out-of-plane waves with a narrow low-frequency range with a peak at 20 kHz.

(a) In-plane displacement (U1)　　　　(b) Out-of-plane displacement (U3)
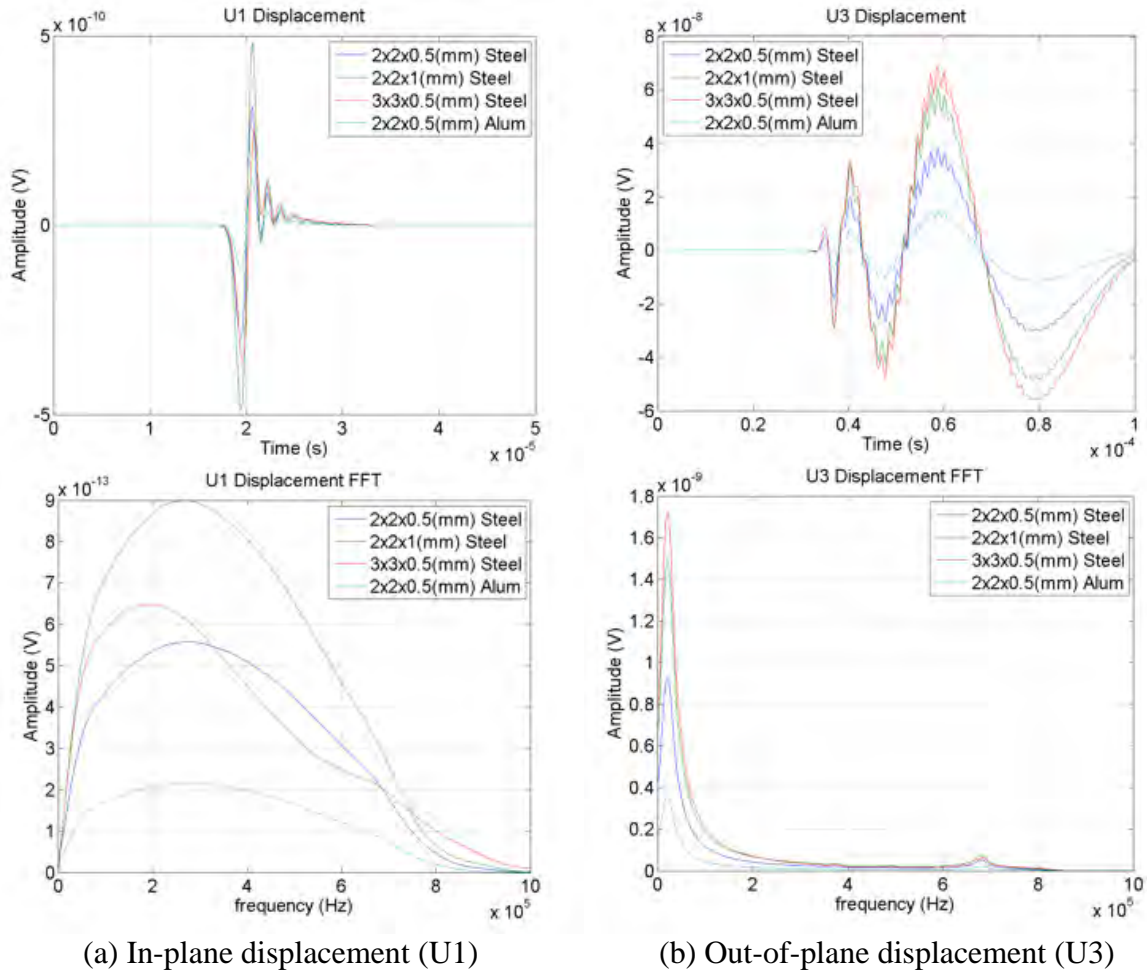
Figure 25. FEM simulation of mini-impactor: (a) in-plane displacement and (b) out-of-plane displacement

The experimental tests used the mini-impactor on an aluminum plate. A thin sheet of aluminum that matched the thickness of the metal tip served the purpose of a shim to allow the whole surface of the impactor tip to impact the aluminum plate (see Figure 24b). Experimental results of a mini-impactor on an aluminum plate showed a frequency range generated up to 500 kHz and peak intensity at 42 kHz (see Figure 26). Compared to the simulation results, the 42 kHz peak was determined to be dominantly from the out-of-plane waves.

Tests of the mini-impactor on the Frame02 panel confirmed that the low-frequency 42 kHz waves can achieve transmission through the internal structure. Figure 27 shows the Frame02 panel test setup with receiver transducers (Mistras R15s) placed on the external skin side and on the C-frame at midpoint along the internal side of the wave path. Test results of the mini-impactor on the Frame02 panel, shown in Figure 28b, clearly show a significant amount of energy propagating into the panel's internal wave path when the excitation was generated using the mini-impactor. Figure 28c clearly shows low-frequency wave intensity loss when the C-frame was disassembled from the panel. Therefore, this setup and excitation technique has high potential for detecting breaks in the frame or other damage along the internal structure wave path.
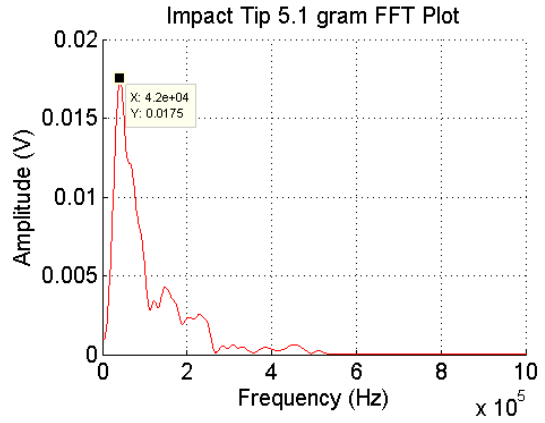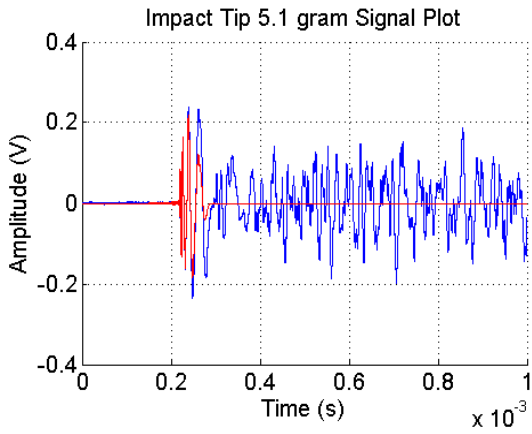
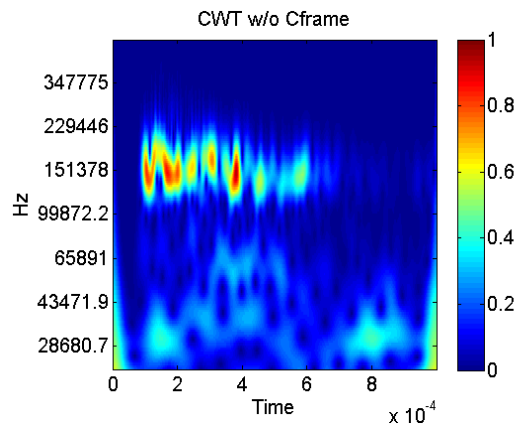**Figure 26. Mini-impactor experiment on aluminum plate test results**
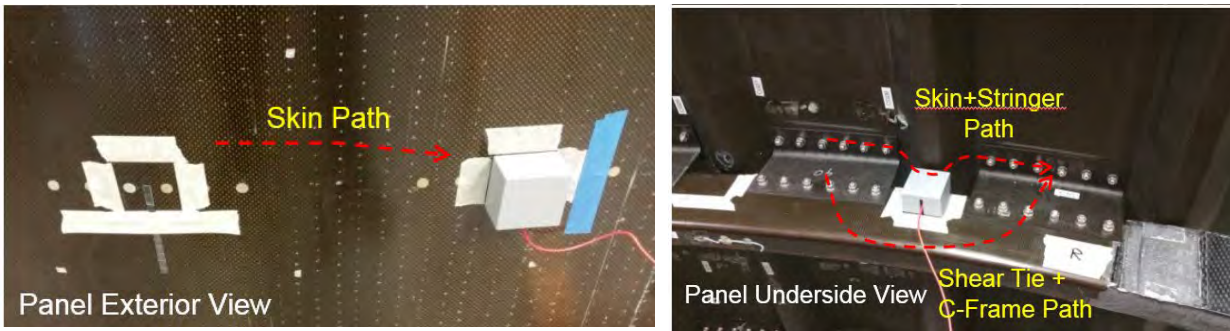
Figure 27. Mini-impactor experiment on Frame02 panel
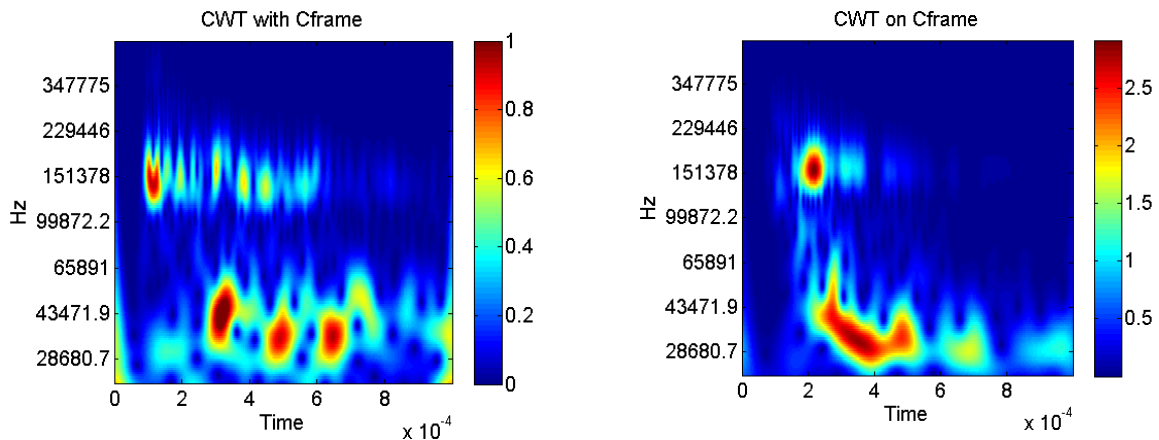
(a) Panel with C-frame, received on skin

(b) Panel with C-frame, received on C-frame

(c) Panel without C-frame, received on skin

Figure 28. Mini-impactor experiment on Frame02 panel results: (a) panel with C-frame, received on skin, (b) panel with C-frame, received on C-frame, and (c) panel without C-frame, received on skin

5. ONGOING AND FUTURE WORK

5.1 Structure Characterization and Assumption Validation

The use of UGWs and the analysis employed in the development of the technique rely on the wave propagation through the given material, and the geometry, assembly, and health condition of the specimen. The characterization of the wave-propagation properties becomes important to understand and better exploit the feature changes, and validate the assumption made to perform the experimental tests.

Phase and group velocity dispersion curves describe the UGW modes with respect to the frequency range. For isotropic plates, it is possible to compute them analytically for simple geometries and materials (homogenous plate) solving the transcendental equation [4]:

$$\frac{\tan(qh)}{q} + \frac{4k^2 p \tan(ph)}{(q^2 - k^2)^2} = 0 \quad \text{for symmetric modes} \tag{3}$$

$$q \tan(qh) + \frac{(q^2 - k^2)^2 \tan(ph)}{4k^2 p} = 0 \quad \text{for antisymmetric modes} \tag{4}$$

When given a composite material, it is possible to compute them analytically for a plate geometry of given thickness and with equivalent material properties. The lay-up and properties of the examined composite panels, summarized in Table 1, have been reduced to a laminate of equivalent thickness and material properties (see Table 4), using a Matlab routine that takes into account the number of plies, orientation, thickness, and material properties of each lamina. The analytical dispersion curves appear in Figure 29.

**Table 4. Material properties of equivalent laminate**

| Property Name	Thickness (mm)	E_x (GPa)	E_y (GPa)	G_{xy} (GPa)	ν	C_L (m/s)	C_T (m/s)
Property Value	2.688	48.895	48.895	16.023	0.254	6079	3165

(a) Group velocity
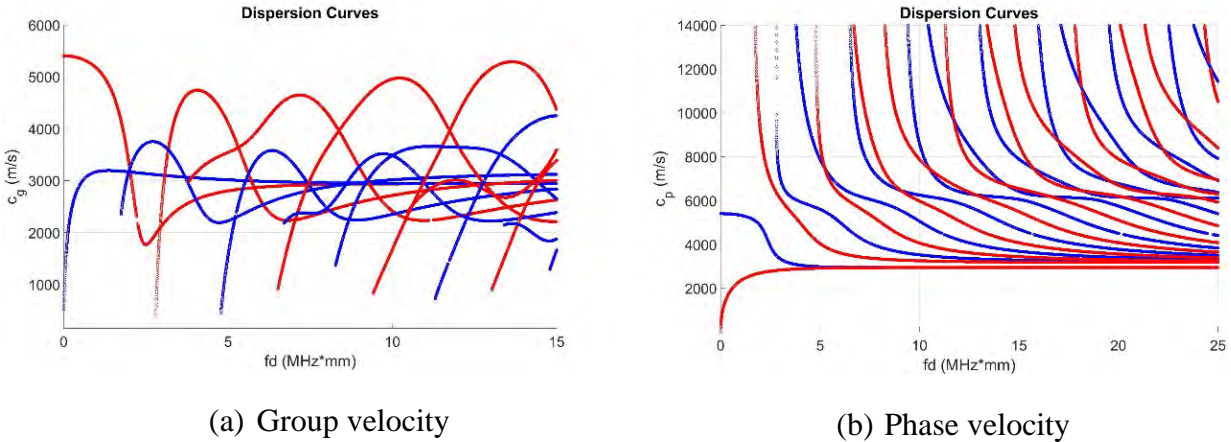
(b) Phase velocity

Figure 29. Dispersion curves for composite plate: (a) group velocity and (b) phase velocity

The analytical solution cannot account for the wave propagation through many interfaces (mainly the higher attenuation), into different angles, and for geometries that are more complex. This can be accounted for using FEM simulations and experimental investigation.

A 2D FFT can be used to extract phase-velocity dispersion curves for a given structure. A multiple input, single output or single input, multiple output configuration is needed, using fixed broadband capacitive air-coupled transducers (BAT, from Microacoustics) for reception and a pulsed laser excitation (Q-switched ND:Yag, 1064 nm, 9 ns duration). Test results for a laser impulse sent along a line of 64 points (nodes) with a 1-mm resolution appear in Figure 30. Similar tests repeated on an aluminum plate appear for purposes of comparison. The time signal on the first point of the line scan, node 1, appear in Figure 31 for two receivers. The respective FFT for one receiver for the A_0 and S_0 gated modes appears in Figure 32.

30
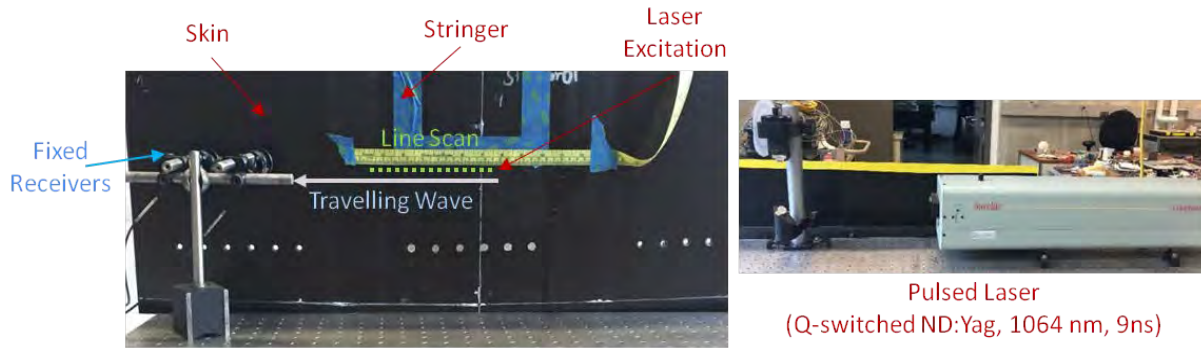
Figure 30. Laser scanning test setup on composite panel

(a) Aluminum plate (b) Composite plate
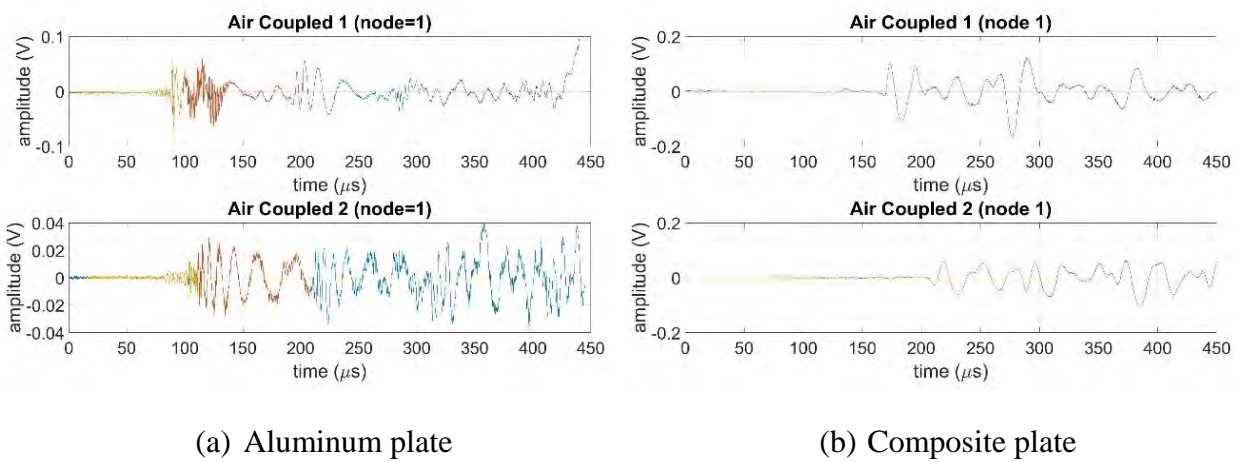
Figure 31. Time signal at node 1 for two air-coupled receivers (top and bottom): (a) aluminum plate and (b) composite plate

(a) Aluminum plate (b) Composite plate
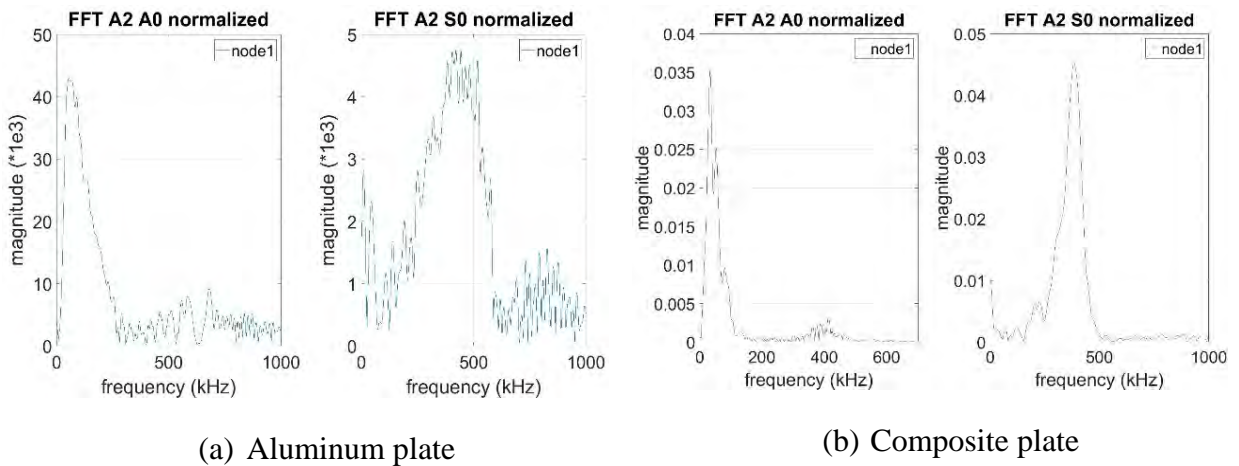
Figure 32. FFT of signal at node 1 for A_0 and S_0 modes: (a) aluminum plate and (b) composite plate

The composite material attenuates the higher frequencies, and the curved and complex structure disturbs the dispersion of the wave packets and interferes within them. By applying a 2D FFT, it is possible to visualize the phase velocity dispersion curves in terms of frequency wavenumber for the multiple modes plotted in Figure 33.

(a) Aluminum plate
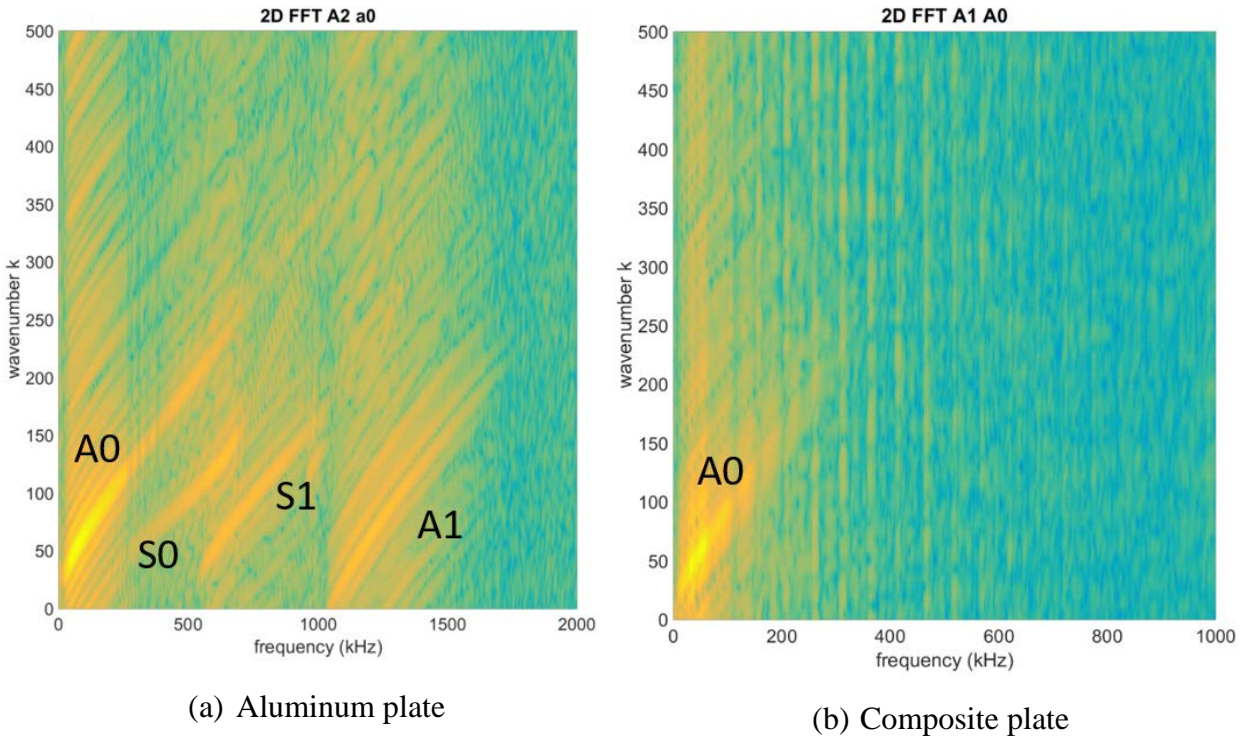
(b) Composite plate

Figure 33. 2D FFT: (a) aluminum plate and (b) composite plate

The composite panel filters out most of the modes, especially at the higher frequencies. Plotting this information in a phase velocity vector, the following dispersion curves appear in Figure 34. Work is underway to improve the phase velocity dispersion curves extraction through gating, windowing, and space-time filtering. Group velocity dispersion curves retrieval is also under study using CWT. A preliminary result confirms the use of the A_0 mode group velocity as 1600 m/s for 170 kHz in the gating of the defect-detection analysis performed and shown in Figure 35d.
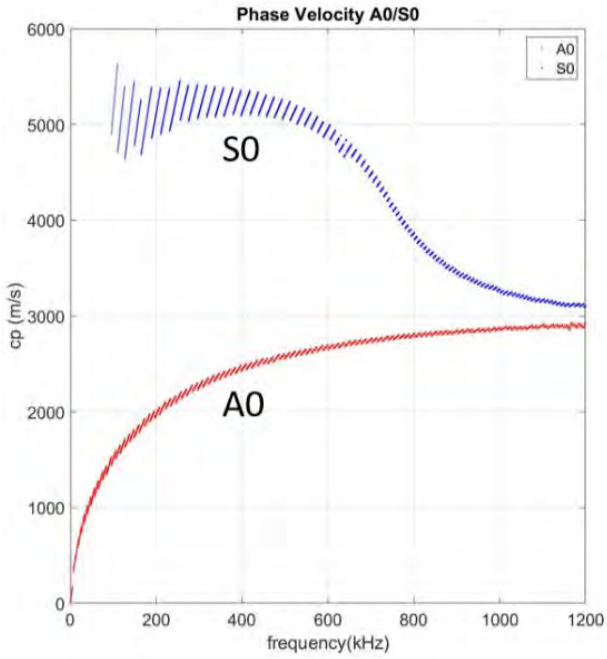
(a) Aluminum plate
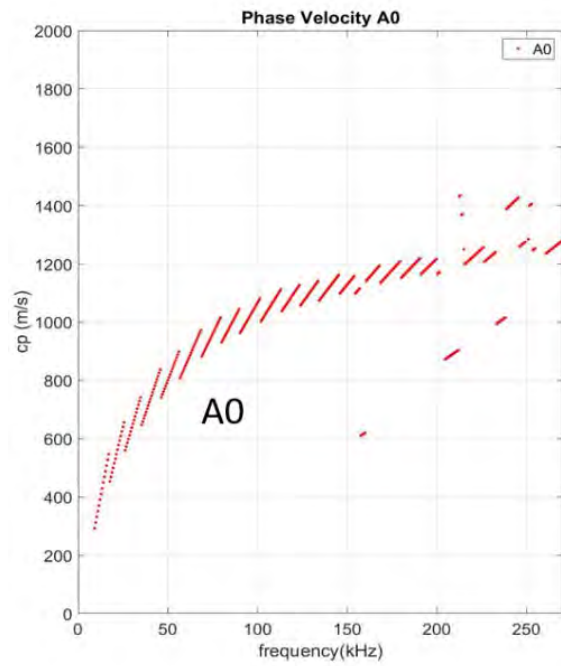
(b) Composite plate

Figure 34. Experimental dispersion curves (phase velocity): (a) aluminum plate and (b) composite plate
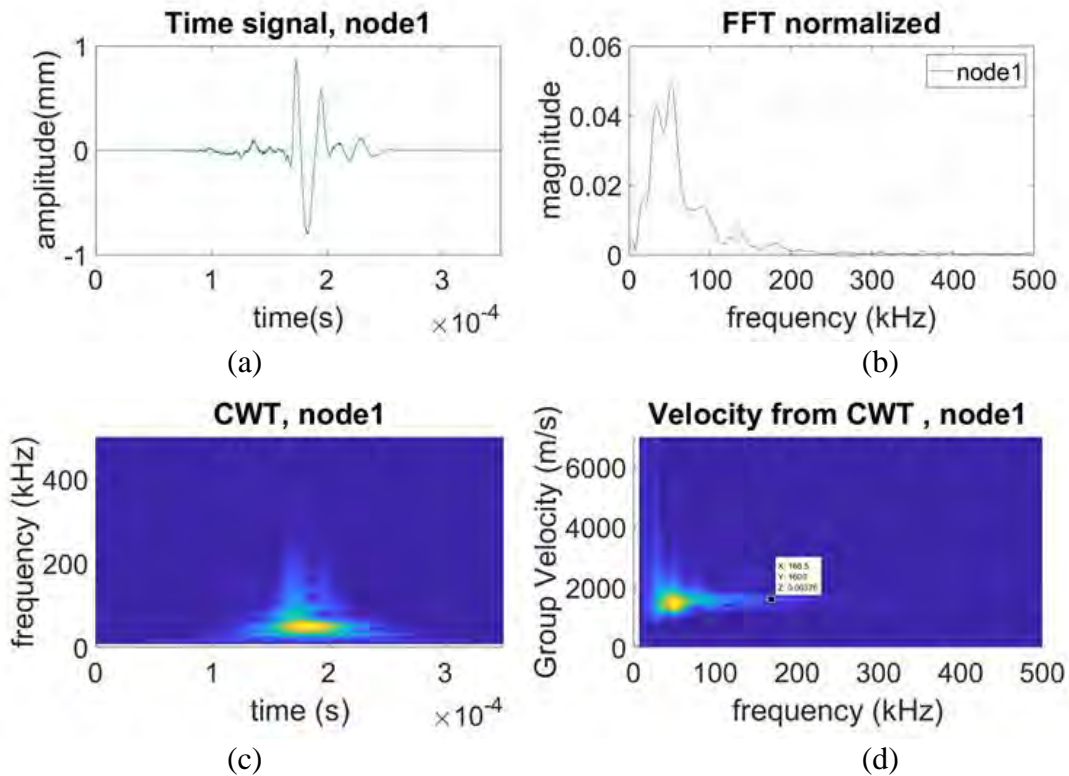
(a)

(b)

(c)

(d)

Figure 35. Composite plate at node 1: (a) gated time signal, (b) FFT of A$_0$ mode, (c) time-frequency CWT, and (d) experimental dispersion curve (group velocity) for A$_0$ mode

5.2 Prototype Development

A laboratory prototype cart designed and built for a field portable system allowed field demonstrations. The scanning assembly appears in Figure 20b.

5.2.1 Automation

Ongoing work will automate the cart scanning by the addition of a position encoder synchronized with the data-acquisition and result display. The objective of automation is to develop a system that renders a B-scan-type output in real time during a scan. The use of the mini-impactor as the wave excitation, and the automation of the impact, are also research subjects under current consideration.

5.3 Residual Strength Estimation from UGW

Estimation of residual strength, explored through UGW measurement when it interacts with damage, seems feasible. Caprino [10] determined residual strength can be predicted based on a notch size in laminated material. By relating UGW results to the size of the damage in composite part, it may be possible to estimate residual strength of the damaged part.

6. CONCLUSION

Non-destructive evaluation damage detection was performed on the composite panels from a previous HEWABI project, with major damage developed in interior structural components of the panels. Ultrasonic guided wave (UGW) transmission through the composite panel parts was examined through manipulation of the panel (e.g., states of assembly and disassembly). From various tests to study wave propagation in internal components, suitable frequencies for each part were determined: approximately 150 kHz for damages in the skin and stringer and approximately 50 kHz for damages in the C-frame and shear ties. R15s transducers were used as actuator and receiver sensors for the contact-based damage detection technique in the 150 kHz range. A more sophisticated prototype developed using air-coupled non-contact transducers for ease of scanning proved beneficial. The general statistical multivariate outlier analysis was applied to both contact and non-contact systems by extracting wave-energy features from different time gates. Both contact and non-contact systems were shown to have good performance in damage detection in the skin and the stringers; skin and stringer combined wave modes assessment gave perfect detection probability with non-contact systems. Damage in the C-frame and shear ties will require lower frequencies of approximately 50 kHz. Phase-velocity and group-velocity dispersion curves for the composite panel parts were obtained through experiments and simulations. This provided a better understanding of UGW propagation through the composite parts for more accurate wave packet gating.

7. REFERENCES

1. Capriotti, M., Kim, H. E., Lanza di Scalea, F., Kim, H. (2017). *Development of an ultrasonic nondestructive inspection method for impact damage detection in composite aircraft structures*. Paper presented at the Proc. SPIE 10169, Nondestructive Characterization and Monitoring of Advanced Materials, Aerospace, and Civil Infrastructure, Denver, CO.

2. Capriotti, M., Kim, H. E., Lanza di Scalea, F., Kim, H. (2017). Non-Destructive Inspection of Impact Damage in Composite Aircraft Panels by Ultrasonic Guided Waves and Statistical Processing. *Materials*, *10*(6).

3. DeFrancisci, G. K. (2013). *High energy wide area blunt impact on composite aircraft structures.* (Thesis) *University of California, San Diego*, CA.

4. Rose J. L., (2004). Ultrasonic waves in solid media. *The Journal of the Acoustical Society of America, 107*(4).

5. Nucera, C., White, S., Chen, Z. M., Kim, H., Lanza di Scalea, F., (2015). Impact monitoring in stiffened composite aerospace panels by wave propagation. *Structural Health Monitoring International Journal, 14*(6), 547–557.

6. Alleyne, D., Cawley, P., (1991). A two-dimensional Fourier transform method for the measurement of propagating multimode signals. *Journal of Acoustic Society of America, 89*(3), 1159–1168.

7. Worden, K., Manson, G., Fieller, N. (2000). Damage detection using outlier analysis. *Journal of Sound and Vibration, 229*(3), 647–667.

8. Bao, J., Shen, Y., Giurgiutiu, V. (2013). *Linear and Nonlinear Finite Element Simulation of Wave Propagation through Bolted Lap Joint.* Presented at the 54th AIAA/ASME/ASCE/AHS/ASC Structures, Structural Dynamics, and Materials Conference, Boston, MA.

9. Yang, J., & Chang, F. K. (2006). Detection of bolt loosening in C–C composite thermal protection panels: I. Diagnostic principle. *Smart Materials and Structures*, *15*(2), 581.

10. Caprino, G. (1983). On the prediction of residual strength for notched laminates. (1983). *Journal of Materials Science*, *18*(8), 2269–2273.